International Journal of Engineering Trends and Technology
ISSN: 2231 – 5381 /doi:10.14445/22315381/IJETT-V70I1P237

Volume 70 Issue 1, 327-347, January, 2022
©2022 Seventh Sense Research Group®

Original Article

Analysis of Effects of Radial Clearance and Unbalance on Vibration Responses of a Rotor-Bearing System

Prashant H. Jain[1,2], Dr. Santosh P. Bhosle[3]

[1]*Research Scholar, Maharashtra Institute of Technology, Aurangabad, Maharashtra, India*
[2]*Assistant Professor, T.P.C.T's College of Engineering, Osmanabad, Maharashtra, India*
https://orcid.org/0000-0002-4501-0419
[3]*Professor and Principal, Maharashtra Institute of Technology, Aurangabad, Maharashtra, India*
https://orcid.org/0000-0003-0636-1723

[1]phjain30@rediffmail.com, [3]spbhosle2001@gmail.com

Abstract *- The objective of this paper is to study and analyze the effects of change in radial clearance of ball bearing under balanced and unbalanced rotor conditions at different speeds and radial loads. In this paper, a rotor-bearing system is modelled, and its vibration responses are simulated for different operating conditions using COMSOL multiphysics software. Two-level full factorial design with four factors (2^4 full factorial design) is used for the design of simulation experiments, and the design is analyzed by using analysis of variance (ANOVA). Four factors, namely disk eccentricity (for balanced/unbalanced rotor), radial clearance, rotor speed and radial load, are used in this study. Root mean square velocities of time waveform in vertical and horizontal directions are considered as vibration response parameters. Minitab software is used to create the factorial designs, ANOVA tables, regression equations and various plots. Response surfaces obtained clearly depict the effects of radial clearance, disk eccentricity, rotor speed and radial load on vibration amplitude. The designed models are significant, with large R-square values (> 99 %). It is also observed that radial clearance has a remarkable effect and radial load has a negligible effect on vibration responses of the rotor-bearing system for the selected range.*

Keywords *- Vibration signal analysis, full factorial design (FFD), COMSOL, radial clearance of bearing, unbalance.*

I. INTRODUCTION

The vibration amplitude of the rotor-bearing system depends on the bearing operating conditions such as rotor speed, radial load, unbalance, misalignment, rotor parameters and bearing parameters. Rotor parameters include rotor length, diameter and material. Bearing parameters include the type of bearing, clearances, pitch diameter, ball diameter, number of balls, bearing material, bearing defects (localized or distributed), etc. Radial clearance is one of the important parameters of ball bearings. Radial clearance is the total radial relative movement between the inner and outer races of bearing. Radial clearance helps to compensate for the thermal expansion of bearing parts. Fig. 1 shows radial clearance of a single row deep groove ball bearing. The amount of radial clearance influences the load distribution in the bearing. The small amount of radial clearance increases excessive pressure on bearing races and rolling elements, which increases bearing wear and ultimately affects the bearing life [1]. But, an increase in radial clearance causes a rise in vibration amplitude. So, it is necessary to choose proper radial clearance of bearing [2]. Usually, radial clearance is an independent parameter. However, at very high speeds (above 21000 rpm), the centrifugal force acting on rolling elements increases the radial clearance [3], [4]. In this study, two-rotor speeds, 2800 rpm and 10200 rpm, are selected. As these speeds are less than 21000 rpm, the effect of centrifugal force on rolling elements is neglected, and therefore radial clearance is considered as an independent parameter. To avoid the occurrence of unwanted vibrations, which may arise due to the critical speed of the rotor, special care is taken while selecting rotor speeds and radial loads so as to keep the rotor speeds away from the critical speeds of the rotor.

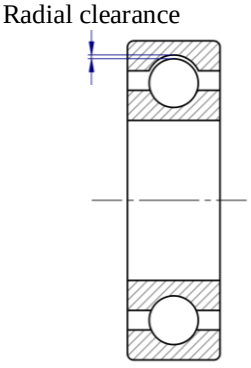

Fig. 1. Radial clearance in a single row deep groove ball bearing.

This is an open access article under the CC BY-NC-ND license (http://creativecommons.org/licenses/by-nc-nd/4.0/)

Unbalance is another main contributor to the vibrations in the rotating types of machinery, which develops synchronous amplitude of vibration. Unbalance is a dependent parameter that depends on the unbalanced mass, speed and eccentricity of unbalanced mass [5]. In this paper, two cases of balancing are considered; the first is the fully balanced rotor with zero eccentricity, and the other is an unbalanced rotor with a 1 mm eccentricity of disk mass.

There is various vibration signal analysis (VSA) techniques commonly used for the diagnosis of faults in the rotor-bearing systems, which include time domain, frequency domain and time-frequency domain analysis. Recently, Jain and Bhosle reviewed the applications of these techniques for rotating types of machinery [6] and bearings [7]. In this present study, time-domain analysis and frequency domain analysis techniques of VSA are used to study the dynamic behaviour of the rotor-bearing system. Root mean square (RMS) velocity obtained from time waveforms in vertical and horizontal directions are used as vibration response parameters. Frequency spectrums are used to study the vibration peaks generated at rotor speed frequencies and critical speed frequencies.

In recent years, many researchers studied the effects of radial clearance and unbalanced rotor-bearing systems by developing mathematical models using Hertzian contact theory. Researchers developed non-linear mathematical models of rotor-bearing systems with different degrees of freedom (dof) models. They considered the nonlinearity of the rotor-bearing system due to clearance and unbalanced. Tiwari et al. [8], [9] studied the effect of radial clearance of ball bearing on balanced rotor [8] and on unbalanced rotor [9]. They showed that a change in internal clearance raises the peak response with an increase in speed. Harsha [10], [11] studied the effects of radial clearance and surface waviness for the balanced rotor. He showed that the instability and chaos in the system increase with speed. He also studied the effects of radial clearance and unbalanced rotor [12]. Changqing and Qingyu [13] studied the effect of radial clearance and surface waviness of ball bearing. They showed that clearance and radial load significantly affect the stability of the system. Upadhyay et al. [14] studied the effect of radial clearance, unbalanced force and rotor speed on bearing vibration. They stated that higher clearance produces more sub-harmonic components at the rotational frequency as compared with lesser clearance. Chen [15] studied the effects of unbalance, clearance and speed on bearing vibration response. Kappaganthu and Natraj [16] studied the effects of clearance, unbalance and stiffness on dynamic stability of the rotor-bearing system. They stated that clearance is an important source of nonlinearity which causes bifurcations and chaos. Nan G. et al. [17] analyzed the effect of speed, clearance and stiffness on the vibration response of the rotor-bearing system. Cheng et al. [18] studied the effects of radial clearance, rotor-stator rubbing, waviness, load, speed and local defects in bearings. Xu et al. [19] studied the effects of radial clearance and radial loads on vibration amplitude of rotor-bearing system. They found that vibration amplitude of ball bearing increases with increase in radial clearance and load. Jain and Bhosle [20] studied the effect of radial load on bearing vibration using time-domain statistical parameters. They stated that with the increase in radial load, the vibration amplitude initially decreases and then increases.

Some researchers analyzed the effects of bearing structure geometry and operating conditions by using finite element analysis (FEA) Software. Kiral and Karagulle [21] studied the vibration response of the bearing structure in dynamic loading conditions using a finite element package IDEAS. They proposed a force model to simulate the effects of localized bearing defects and used time and frequency domain analyses for diagnostic purposes. They performed a similar analysis under the action of unbalanced forces [22]. Liu et al. [23] used the explicit dynamic FEA method to study the effects of defect shape, radial load and speed on vibration response. They stated that vibration response is greatly increased due to localized defects followed by shaft speed and load. Singh et al. [24] simulated and analyzed the effects of outer race defects (ORDs) in ball bearing using FEA software LS-DYNA. Tyagi and Panigrahi [25] modelled and simulated the effects of crack on the outer race of the ball bearing using FEA software ANSYS. Nabhan et al. [26] modelled and simulated the effects of ORDs using FEA software ABAQUS. Yang et al. [27] modelled and simulated the effects of inner and outer race defects using ABAQUS software.

Some researchers used DOE and response surface methodology (RSM) to analyze and predict the dynamic responses of rotor-bearing systems under the influence of different geometric and operating conditions. Kankar et al. [28] mathematically modelled and simulated the effects of four factors, namely, radial clearance and surface waviness, on the inner race, outer race and ball. They used 2^4 full factorial designs (FFD) and RSM to analyze their effects on vibration response. They used displacement (in μm) of a frequency spectrum in vertical and horizontal directions as a response variable. Patil et al. [29] used Box Behnken design and RSM to study the effect of defect size of ORD, inner race defect (IRD) and ball defect (BD), speed and load on vibration response of a ball bearing. They used kurtosis as a response variable and found that kurtosis is more sensitive to the defect size. Kankar et al. [30] studied the effects of speed and spalls on the inner race, outer race and ball. They used fractional factorial DOE (2^{4-1}) and RSM to analyze their effects on vibration response. They used acceleration (in gRMS) of a frequency spectrum in vertical and horizontal directions as a response variable. Kankar et al. [31] also incorporate the influence of cracked and un-cracked rotors in their later study. Jamadar and Vakharia [32] studied the effect of roller defect size, unbalance, radial load, axial load, radial clearance, speed, number of rollers and grease viscosity. They used Taguchi's L_{27} design to reduce the

number of experiments and used acceleration (in m/s^2) of the frequency spectrum as a response variable. Yucel and Saruhan [33] studied the effect of shaft speed, coupling type and disk location on the vibration response of the rotor-bearing system. They used Taguchi's L_9 design and used velocity RMS (in m/s) of time waveform as a response variable. Boumahdi et al. [34] used 2^5 FFD to study the effect of speed, radial load, spall size, sensor position and frequency range on vibration amplitude. They used acceleration RMS (in m/s^2) of time waveform as a response variable. Patil and Jadhav [35] used a dynamic model using Dimensional Analysis (DA) to predict the effects of radial clearance, unbalance and rotor speed of the rotor-bearing system. They used 2^3 FFD for analysis and used velocity amplitude (in mm/s) of the frequency spectrum as a response variable. Patra et al. [36] used a mathematical model to predict the effects of radial clearance, speed and load on the vibration amplitude of a cylindrical roller bearing. They used a mixed factorial design with 24 runs and used acceleration amplitude (in m/s^2) of the frequency spectrum as a response variable. Singh and Harsha [37] used RSM for vibration response based fault dynamics of cylindrical roller bearing. They studied the effects of load, speed and defect size on vibration response. They observed that a small variation of speed significantly increases vibration amplitude, while a change in load has less impact on vibration amplitude. Mishra and Jalan [38] studied the effects of speed, load and type of defect (IRD, ORD and combination of BD and ORD) on ball bearing vibration. They used 3^3 FFD along with RSM for analysis and used acceleration amplitude (in m/s^2) of time waveform in vertical and horizontal directions. Patil et al. [39] studied the effects of speed, load and misalignment (parallel and angular) on the vibration amplitude of a rotor-bearing system. They used 3^3 FFD for both parallel and angular misalignment conditions. They used acceleration RMS (in m/s^2) of time waveform as a response variable. They stated that change in load has less impact on vibration amplitude.

The literature review revealed that most of the researchers used MATLAB software for mathematical modelling and simulation of combined effects of radial clearance and unbalance on vibration response of the rotor-bearing system. It is also seen that few researchers used finite element analysis (FEA) software for modelling and simulation of faults in bearings. In this literature, it is also observed that the effects on bearing vibration due to critical speeds are not taken into consideration. This inspires the authors to focus on the use of FEA software to study the effects of change in radial clearance of bearing, unbalance of rotor-bearing system, change in radial load and speed on vibration response of the rotor-bearing system by considering the critical speeds. In this paper, COMSOL multiphysics 5.6 software is used for modelling and simulation of rotor-bearing system vibration due to various factors, Matlab R2020b is used to calculate the vibration response parameter RMS velocity by processing the data, and Minitab 19 statistical software is used for 2^4 full factorial DOE, ANOVA, regression modelling and response surface analysis. The methodology used for 2^4 FFD for vibration responses is shown in fig. 2. The results obtained provide theoretical support to understand the effects of various factors on the vibration of a rotor-bearing system in real situations.

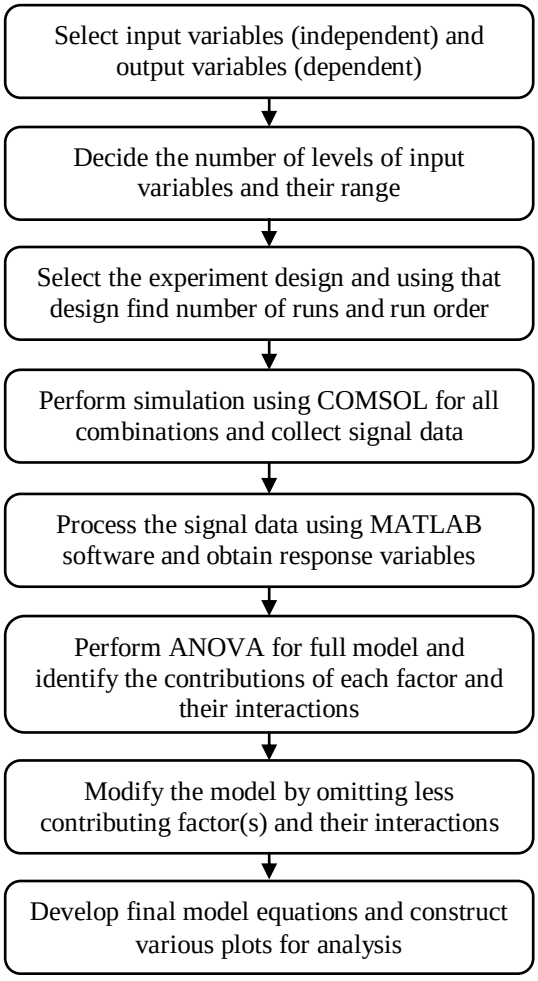

Fig. 2. Methodology for 2^4 full factorial designs for vibration response

II. ROTOR-BEARING SYSTEM DESIGN AND SIMULATION

A. Rotor-bearing system design

In order to study the effects of various factors on vibration responses of the rotor-bearing system, a rotor-bearing system is modelled using COMSOL multiphysics software. This system has a flexible rotor with a rigid disk mounted at the centre. The rotor is simply supported on two single row deep groove ball bearings of number 6205 and is subjected to gravitational force. Ball-bearing 6205 has a wide range of applications in industrial machinery, automation, power tools, motorcycles, electric motors, etc. A schematic

diagram of the setup of the rotor-bearing system considered for the study is shown in Fig. 3. The details of the rotor-bearing system parameters are shown in Table I.

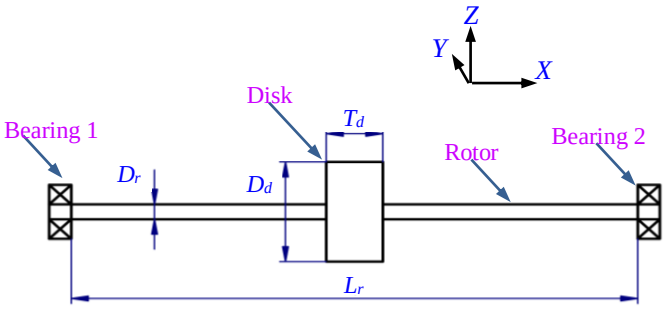

Fig. 3. Schematic diagram of the rotor-bearing system

TABLE I
DETAILS OF ROTOR-BEARING SYSTEM

Rotor and Disk Details	
Rotor diameter (D_r)	25 mm
Rotor length (L_r)	1000 mm
Disk diameter (D_d)	200 mm
Disk thickness (T_d)	26.12 mm, 110.09 mm
Disk eccentricity (E_d)	0, 1 mm
Density of rotor and disk materials (ρ)	7850 kg/m^3
Young's modulus (E)	200 GPa
Poisson's ratio (ν)	0.3
Rotor and Disk weight (W)	100 N, 300 N
Rotor speed (N_r)	2800 rpm, 10200 rpm
Bearing Details	
Bearing model	Deep groove ball bearing 6205
Nominal bore diameter (d)	25 mm
Nominal outside diameter (D)	52 mm
Ball diameter (D_b)	7.94 mm
Pitch diameter (P_d)	39.04 mm
Outer race diameter (D_o)	46.98 mm
Inner race diameter (D_i)	31.10 mm
Outer race groove radius (r_o)	4.208 mm
Inner race groove radius (r_i)	4.208 mm
Number of balls (n)	9
Contact angle (α)	0^0
Young's modulus of bearing material (E)	200 GPa
Poisson's ratio of bearing material (ν)	0.3
Radial load on each bearing (W_r)	50 N, 150 N

In this study, the beam rotor interface of COMSOL multiphysics software is used to simulate vibrations of the rotor-bearing system. This interface uses a 3D Timoshenko beam element and supports geometrically linear analysis. The beam rotor approximates the rotor as a 1-dimensional beam by representing the axis of the rotor as a line, and mounting components are set to be as a point condition. The elements in the beam rotor are based on Timoshenko theory having 6 dof (3 displacements and 3 rotational motions). In a beam rotor, the rotor is considered a flexible beam and the disk is considered rigid. Beam rotor interface allows only bending vibrations and suppresses the axial and torsional vibrations; hence it is less time consuming [40].

In this study, the bearing contact stiffness coefficients K_{zz} and K_{yy} in both directions (vertical Z and horizontal Y) are assumed to be linear (constant) and the same in both directions. Fig. 4 shows linear stiffness coefficient K obtained by using COMSOL software for 1 and 53 microns of radial clearances on 6205 balls bearing. It is seen that there is not much effect of change in radial clearance on stiffness coefficient of bearing. Stiffness coefficients are constant for a whole time duration of 0.2 seconds. These stiffness coefficient values depend on radial clearance, bearing geometry and bearing material; and not on load and speed. The analytically calculated value of linear stiffness coefficient K for 6205 ball-bearing using a method mentioned by Harris [41] is $7.819265042099 \times 10^9$ N/m. [Refer Appendix A for calculation of linear bearing stiffness coefficient K]. This calculated value of the stiffness coefficient is slightly different from the values obtained by using COMSOL software. This is because, in analytical calculations, radial clearance of bearing is not considered.

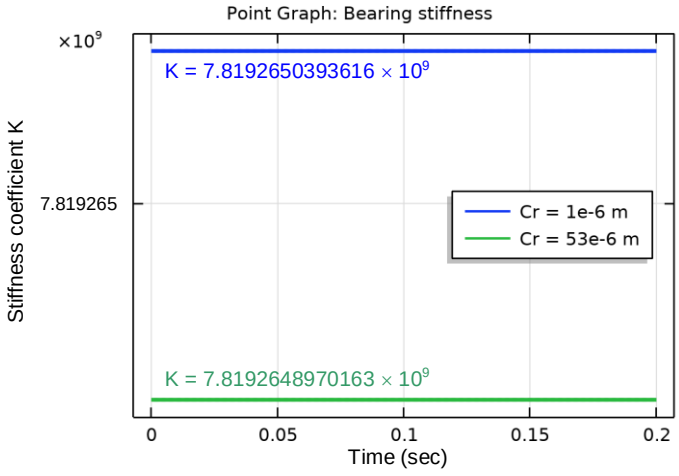

Fig. 4. Linear bearing stiffness coefficient K for bearing 6205 using COMSOL software

B. Selection of range of input variables (factors)

a) Disk eccentricity **(E_d):** To study the effect of unbalancing, two cases of the rotor are considered. In the first case, the rotor is fully balanced with zero eccentricity of masses, and in the other case, the rotor is unbalanced with 1 mm eccentricity of disk mass.

b) Radial clearance **(C_r):** According to International Organization for Standardization (ISO) standard 5753, there are five classes of radial clearance of deep group ball bearings, namely C2, CN (Normal), C3, C4 and C5. For 6205 deep groove ball bearing has 25 mm bore diameter, five classes of radial clearances are shown in Table II. In this paper, the lowest and highest values of radial clearances (1 μm and 53 μm) are selected for a study of their effects on bearing vibration.

TABLE II
RADIAL CLEARANCE RANGE OF 6205 BALL BEARING AS PER ISO 5753

Bore diameter in mm		Radial clearance in microns (μm)									
(d)		(C2)		(CN)		(C3)		(C4)		(C5)	
>	≤	Min.	Max.	Min.	Max.	Min.	Max.	Min.	Max.	Min.	Max.
24	30	**1**	11	5	20	13	28	23	41	30	**53**

c) Radial load **(W_r):** In this study, radial loads acting on each bearing (W_r) are considered in two levels as 50 N and 150 N. [Refer Appendix B for calculation of radial loads on each bearing W_r].

d) Rotor speed **(N_r):** Critical speed of the rotor is a speed that corresponds to the natural resonant frequency of the rotor. It depends on rotor and disk geometry, their material properties and the kind of bearing support. At critical speeds, the rotor vibrates with high amplitude. Therefore, in order to avoid high vibration, the rotor should be avoided to run at critical speeds. Hence, in this study, first, the critical speeds of the rotor-bearing system are obtained by analytical method, by using Dyrobes simulator and COMSOL simulator. Table III shows the critical speeds obtained by using these methods for different radial loads. [Critical speeds of rotor obtained for the selected radial loads and radial clearances are given in appendix C]. It is seen that as there is not much difference in the values of stiffness coefficients (K) for different values of radial clearances (C_r), critical speeds are almost the same for different values of radial clearances. After finding the critical speeds for each load condition, the rotor speeds are selected as 2800 rpm and 10200 rpm. These speeds are away from the critical speeds of the rotor. Thus, unwanted vibrations due to critical speeds are avoided. Fig. 5 shows the mode shape 1 and Campbell plot obtained from the Dyrobes simulator for a rotor-bearing system having radial clearance 1 micron and subjected to 50 N radial loads on each bearing. In this Campbell plot, the excitation line cuts the natural frequency curves at 1428 rpm and 7709 rpm, which represent the critical speeds of the rotor. Fig. 6 shows the Campbell plot obtained from the COMSOL simulator for the same case. In this Campbell plot, the excitation line cuts the natural frequency curves at 150 rad/s and 810 rad/s, which corresponds to critical speeds 1428 rpm and 7709 rpm, respectively. In both fig. 5 and fig. 6, the backward whirl curve of the first frequency curve is hidden below the forward whirl curve. The critical speeds obtained by the analytical method slightly differ from the critical speeds obtained by using Dyrobes and COMSOL simulators because, as an analytical method, the stiffness coefficients of the bearings are not considered. [Refer to Appendix D for calculation of critical speed of rotor by analytical method].

TABLE III
CRITICAL SPEEDS OBTAINED BY ANALYTICAL METHOD AND BY SIMULATORS

Radial load (W_r) in Newton	Critical speeds of a rotor in rpm (Hz)		
	By Analytical Method	By Dyrobes Simulator	By COMSOL Simulator
50	1385.16 (23.09) ---	1428 (23.8) 7709 (128.48)	1428 (23.8) 7709 (128.48)
150	759.03 (12.65) ---	766 (12.75) 4096 (68.27)	766 (12.75) 4096 (68.27)

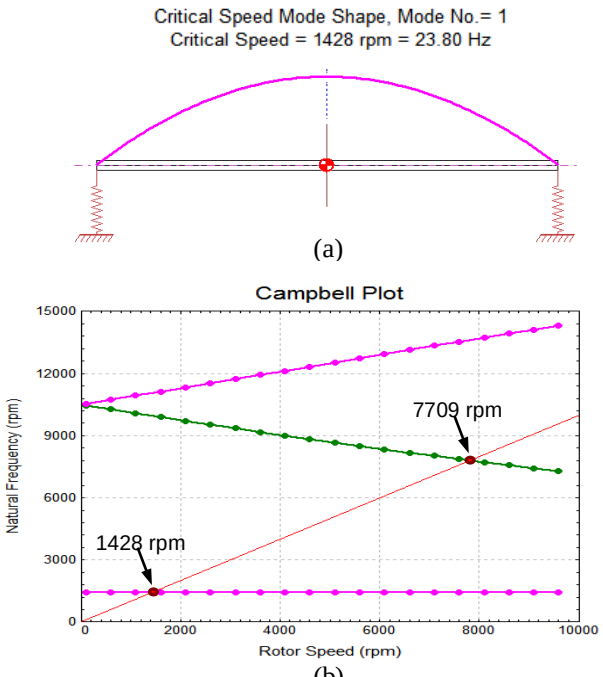

Fig. 5. (a) Mode shape 1 and (b) Campbell plot for a rotor-bearing system using Dyrobes simulator (For C_r = 1 μm and W_r = 50 N)

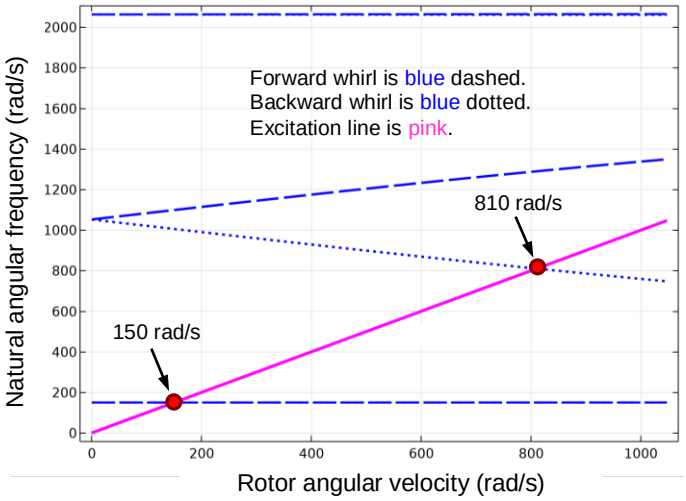

Fig. 6. Campbell plot for rotor-bearing system using COMSOL simulator (For C_r = 1 μm and W_r = 50 N)

C. Design of Experiments (DOE) with Two-level Full Factorial Design (FFD)

Factorial designs are commonly used in experiments to study the joint effects of several input factors on the output response. Input variables (factors) are the independent variables, and output variable (response) is the dependent variable. Response surface is used to describe the surface, which represents the output variable when input variables vary within a specified range. In DOE, the factorial designs are broadly classified as full factorial design and fractional factorial design. In this paper, 2 levels of full factorial design with 4 factors (2^4) is used for the design of simulation experiments for a rotor-bearing system. The input factors considered for DOE are disk eccentricity (for balanced/ unbalanced rotor), radial clearance, rotor speed and radial load; and the output factors are the vibration amplitude RMS velocity in vertical and horizontal directions. Table IV shows DOE factors with coded and uncoded levels.

TABLE IV
DOE FACTORS FOR 2^4 FFD

Factors	Symbol	Unit	Coded Levels		Uncoded Levels	
Disk eccentricity	E_d	mm	–1	+1	0	1
Radial clearance	C_r	μm	–1	+1	1	53
Rotor speed	N_r	rpm	–1	+1	2800	10200
Radial load	W_r	N	–1	+1	50	150

D. Simulation using COMSOL multiphysics software

To study and analyze the effects of change in radial clearance of ball bearing under balanced and unbalanced rotor conditions at different speeds and radial loads, the designed rotor-bearing system (as mentioned in session II-A) is simulated for vibration analysis using COMSOL multiphysics software.

In this simulation, a parametric sweep is performed for all combinations of 4 factors (disk eccentricity, radial clearance, rotor speed and radial load) which include 2 levels of each factor. Therefore, total runs are 2^4 = 16 runs. Parametric sweep is performed in the same order as shown in Table IV. The run order of experiments is given in Table V. For each run, time-dependent analysis is carried out for a time duration of 0.2 seconds with a time step of 0.0002 seconds, i.e. with a 5000 Hz sampling rate. This sampling rate satisfies the condition of the Nyquist theorem, which states that the sampling rate should be more than or equal to twice the highest frequency component of the signal. In this study, the highest frequency is the rotor speed frequency (170 Hz) at a maximum speed of 10200 rpm. Using COMSOL software, for each run, various graphs are obtained, such as orbit plots at left bearing and at the disk, time waveforms in vertical (Z) and horizontal (Y) directions which include displacement vs time, velocity vs time, acceleration vs time, and frequency spectrums in vertical and horizontal directions which include Fourier coefficient vs frequency. For further analysis, the obtained signal data of time waveforms (velocity vs time) are transferred to MATLAB software, and in MATLAB, various statistical parameters like Peak, Peak to Peak, RMS, Crest factor, Skewness, Kurtosis, etc. are obtained. Out of these parameters, RMS velocity (*Vrms*) of time waveforms in vertical and horizontal directions are considered as vibration responses for analysis. RMS is the square root of the mean of squares of a signal. It is the measure of the overall vibration level of the signal [42]. RMS is given by

$$\text{Root Mean Square (RMS)} = \sqrt{\frac{1}{N}\sum_{i=1}^{N}(x_i)^2} \qquad (1)$$

where x_i = Instantaneous signal amplitude and N = No. of samples taken within the signal

The obtained values of simulated vibration responses in vertical and horizontal directions in RMS Velocity (in mm/s) for 16 runs are shown in Table V.

III. RESULTS AND DISCUSSION

A. Orbit Plots, Time waveforms and Frequency Spectrums of Rotor-Bearing System

Fig. 7 and fig. 8 shows orbit plots, time waveforms and frequency spectrums in a vertical direction at the left bearing for balanced and unbalanced rotors of the rotor-bearing system.

From the orbit plot of a balanced rotor (E_d = 0), as shown in fig. 7 (a), it is observed that the centre of the rotor displaces in a downward direction due to the weight of rotor and disk (W) and starts vibrating below its initial position. But, in the case of the unbalanced rotor (E_d = 1 mm), as shown in fig. 8 (a), due to centrifugal force, the centre of the rotor starts rotating about its initial position.

TABLE V
SIMULATION DESIGN MATRIX AND VIBRATION RESPONSES

Run Order	Uncoded factors				Coded factors				Vertical RMS Velocity	Horizontal RMS Velocity
	E_d	C_r	N_r	W_r	E_d	C_r	N_r	W_r	*Vrms(V)*	*Vrms(H)*
1	0	1	2800	50	–1	–1	–1	–1	0.344	0.0875
2	0	1	2800	150	–1	–1	–1	+1	0.2839	0.0518
3	0	1	10200	50	–1	–1	+1	–1	0.3409	0.1587
4	0	1	10200	150	–1	–1	+1	+1	0.2845	0.0954
5	0	53	2800	50	–1	+1	–1	–1	3.9584	6.6405
6	0	53	2800	150	–1	+1	–1	+1	3.9324	8.4583
7	0	53	10200	50	–1	+1	1	–1	3.9242	6.1524
8	0	53	10200	150	–1	+1	+1	+1	4.1583	6.0749
9	1	1	2800	50	+1	–1	–1	–1	0.7394	1.259
10	1	1	2800	150	+1	–1	–1	+1	0.7268	1.366
11	1	1	10200	50	+1	–1	+1	–1	6.278	10.3722
12	1	1	10200	150	+1	–1	+1	+1	6.2922	13.3932
13	1	53	2800	50	+1	+1	–1	–1	21.5597	24.9419
14	1	53	2800	150	+1	+1	–1	+1	20.1193	23.7609
15	1	53	10200	50	+1	+1	+1	–1	179.2253	221.9891
16	1	53	10200	150	+1	+1	+1	+1	173.6035	207.108

From time waveforms of the balanced rotor (E_d = 0), as shown in fig. 7 (b) and (c), it is clearly seen that the peaks are found at intervals of 0.07836 seconds which corresponds to the critical speed frequency (f_c) 12.76 Hz (i.e. 766 rpm). Fig. 7 (d) shows the frequency spectrum with a peak at f_c. As there is no excitation frequency other than critical speed frequency present in the system, the critical speed frequency of rotor f_c can be easily calculated from the time waveforms.

Fig. 8 (b) and (c) shows the time waveforms for unbalanced rotors (E_d = 1 mm). From these figures, it is difficult to find the critical speed frequency present in the system, as unbalance of the rotor adds rotor rotational frequency f_r and makes the system unstable, as shown in fig. 8 (d). It is observed from the time waveforms are shown in fig. 7 and 8 that the vibration amplitude (velocity in mm/s) increases with the presence of unbalance in the system.

From frequency spectrums of the balanced rotor (E_d = 0), it is observed that no peaks are found at rotor rotational frequency f_r for any value of C_r, N_r and W_r. For C_r = 1 μm, there are no significant amplitude peaks found at any speed N_r and at any load W_r (refer fig. 9 (a) and (b)). For C_r = 53 μm, at higher values of load W_r, peaks are found at critical speed frequency f_c and not at rotor rotational frequency f_r (refer fig. 9 (c) and (d)). Frequency peak amplitude changes slightly with W_r but absolutely not with N_r.

From frequency spectrums of unbalanced rotors (E_d = 1 mm), it is observed that peaks are found at rotor rotational frequency f_r for all values of C_r, N_r and W_r. For C_r = 1 μm, peaks are clearly seen at rotor rotational frequency f_r and critical speed frequency f_c for all values of rotor speed N_r and radial load W_r (refer fig. 10 (a) and (b)). For C_r = 53 μm, vibration amplitude increases, and it becomes difficult to find the rotor rotational frequency and critical speed frequency in frequency spectrums (refer fig. 10 (c)). From the frequency spectrums, it is observed that an unbalanced rotor becomes more unstable with an increase in clearance, speed and load. For unbalanced rotors, at low clearance, the only dominant frequencies are the synchronous frequencies at f_c and f_r, and with the increase in clearance, the non-synchronous frequencies increase.

B. Analysis of Vibration Response in Vertical Direction using ANOVA and Various Plots

To investigate the effects of various factors on vibration response of the rotor-bearing system in the vertical direction, first using ANOVA, factorial regression models are developed for the vibration responses obtained through two-level FFD, and then various plots are used for the analysis of the vibration responses.

a) ANOVA for Full Model

A summarized ANOVA table for the full model of vibration response in the vertical (Z) direction is given in Table VI, which shows the effect estimates, sums of squares, and the percentage contribution of each term and their interactions. Percentage contribution of each term shows that vibration amplitude is greatly affected by radial clearance (18.79 %) followed by disk eccentricity (18.42 %) and rotor speed (12.51 %). The radial load has a negligible effect on vibration amplitude.

TABLE VI
EFFECT ESTIMATE SUMMARY FOR FULL MODEL

Model Terms	Effect Estimates	Sum of Squares	Percent Contribution
E_d (A)	48.91	9570.59	18.42
C_r (B)	49.4	9761.02	**18.79**
N_r (C)	40.31	6498.09	12.51
W_r (D)	–0.8711	3.04	0.01
E_d*C_r	45.72	8360.88	16.10
E_d*N_r	40.26	6482.85	12.48
E_d*W_r	–0.894	3.20	0.01
C_r*N_r	37.53	5634.00	10.85
C_r*W_r	–0.8424	2.84	0.01
N_r*W_r	–0.4864	0.95	0.00
E_d*C_r*N_r	37.48	5619.44	10.82
E_d*C_r*W_r	–0.9235	3.41	0.01
E_d*N_r*W_r	–0.5523	1.20	0.00
C_r*N_r*W_r	–0.494	1.00	0.00
E_d*C_r*N_r*W_r	–0.5581	1.20	0.00

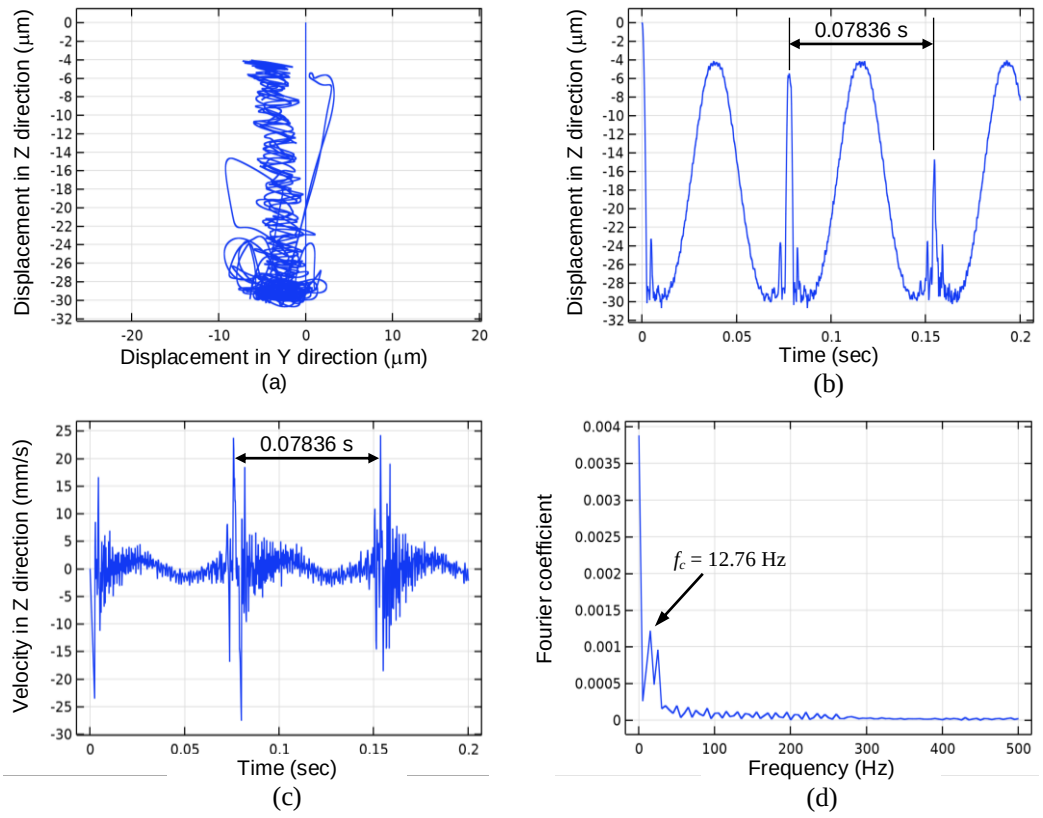

Fig. 7. (a) orbit plot, (b) time waveform (Displacement in Z direction vs. time), (c) time waveform (Velocity in Z direction vs. time), and (d) frequency spectrum (Fourier coefficient in Z direction vs. frequency) at left bearing for balanced rotor with E_d = 0 mm, C_r = 53 μm, N_r = 10200 rpm, W_r = 150 N.

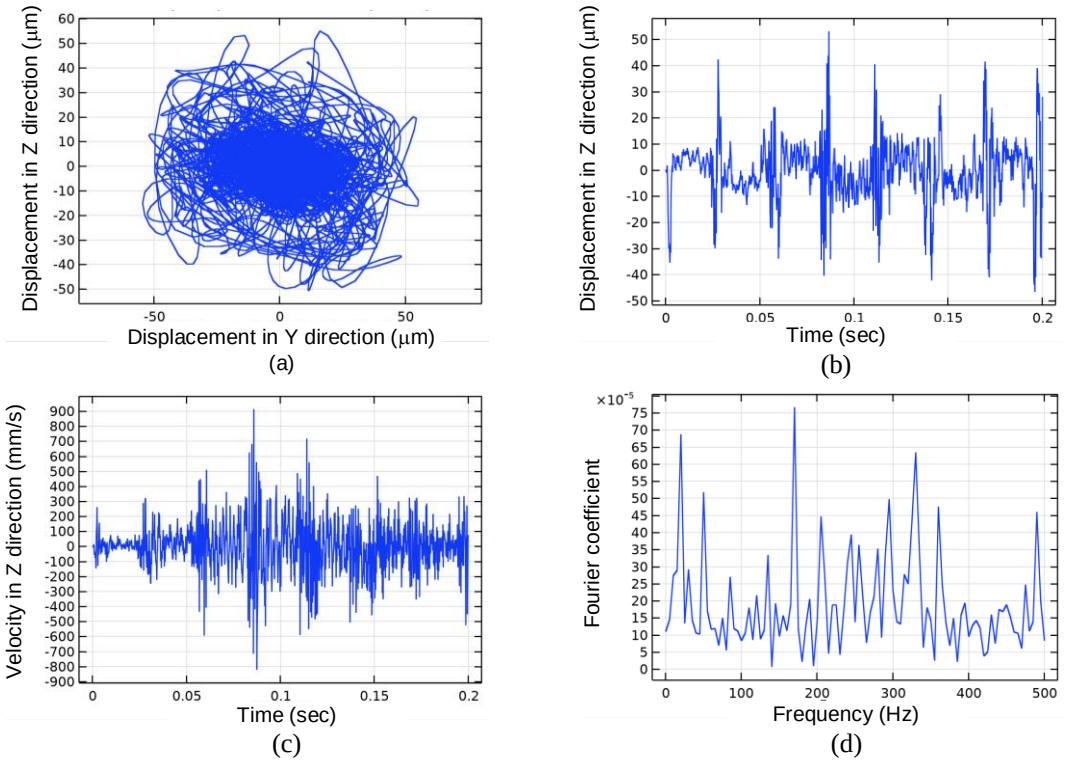

Fig. 8. (a) orbit plot, (b) time waveform (Displacement in Z direction vs. time), (c) time waveform (Velocity in Z direction vs. time), and (d) frequency spectrum (Fourier coefficient in Z direction vs. frequency) at left bearing for unbalanced rotor with E_d = 1 mm, C_r = 53 μm, N_r = 10200 rpm, W_r = 150 N.

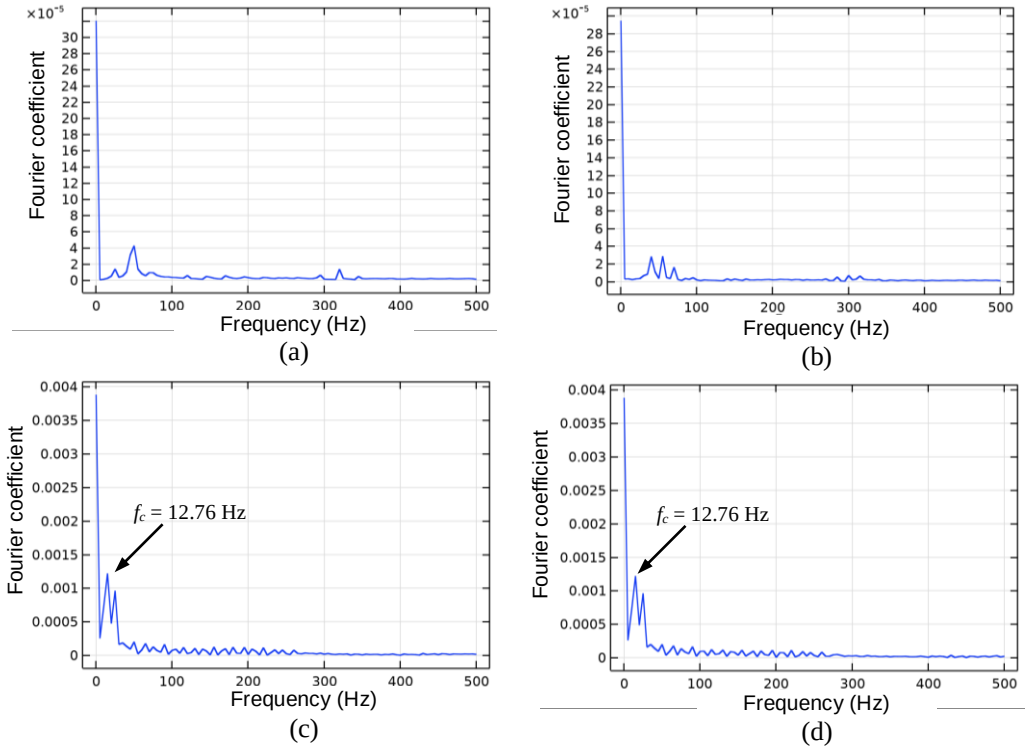

Fig. 9. Frequency spectrums in vertical direction at left bearing for balanced rotor and (a) for C_r = 1 μm, N_r = 2800 rpm, W_r = 50 N, (b) for C_r = 1 μm, N_r = 10200 rpm, W_r = 150 N, (c) for C_r = 53 μm, N_r = 2800 rpm, W_r = 150 N and (d) for C_r = 53 μm, N_r = 10200 rpm, W_r = 150 N

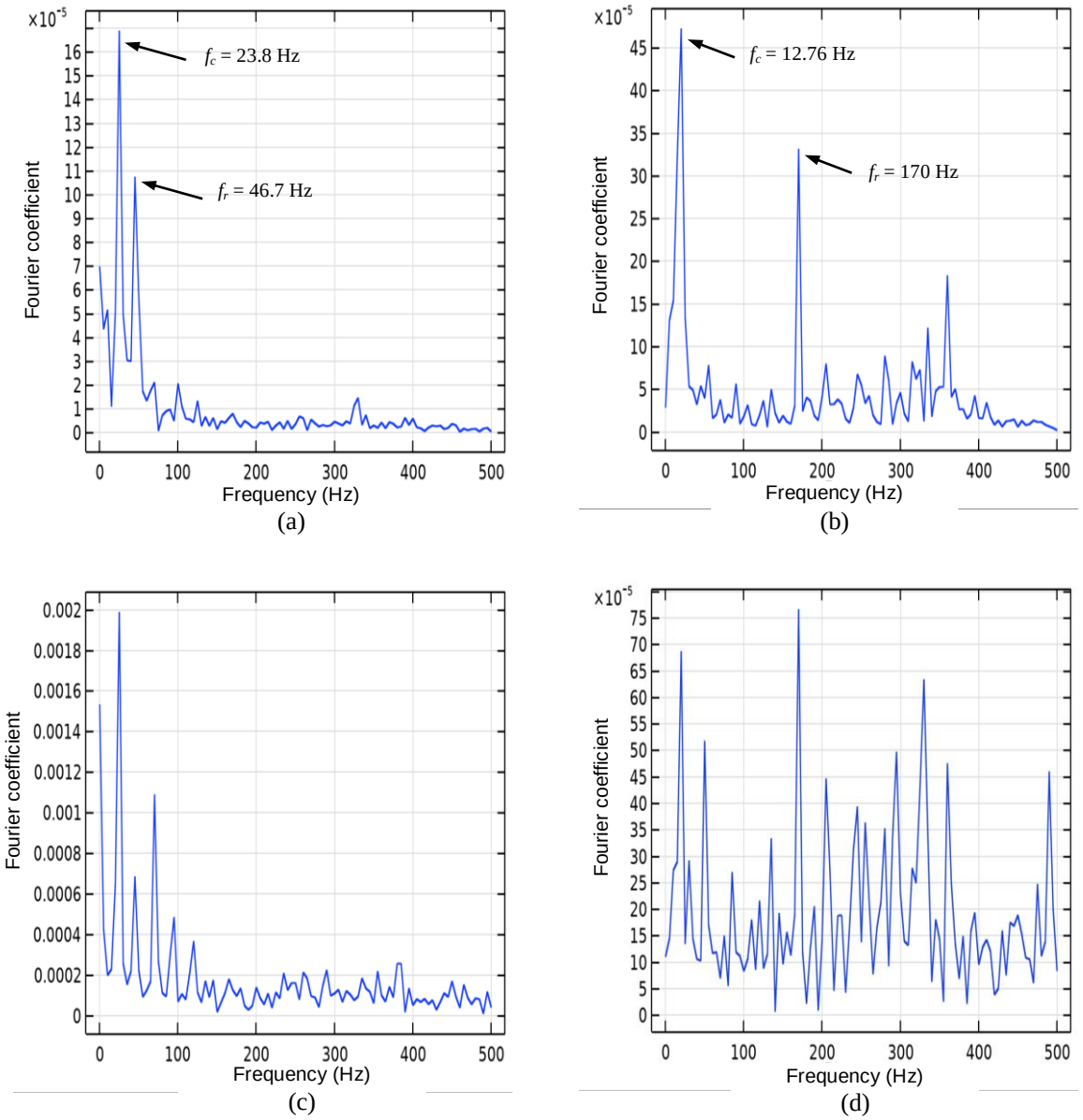

Fig. 10. Frequency spectrums in vertical direction at left bearing for unbalanced rotor and (a) for C_r = 1 µm, N_r = 2800 rpm, W_r = 50 N, (b) for C_r = 1 µm, N_r = 10200 rpm, W_r = 150 N, (c) for C_r = 53 µm, N_r = 2800 rpm, W_r = 50 N and (d) for C_r = 53 µm, N_r = 10200 rpm, W_r = 150 N

b) Pareto Chart and Normal Probability Plot for Full Model

The Pareto chart and normal probability plot of all effects of the full model for 95% confidence level are shown in fig. 11 (a) and (b). In the Pareto chart, significant terms are above the limiting line, and in a normal plot, significant points are away from the reference line as shown. Both the figures show that the terms disk eccentricity (A), radial clearance (B), rotor speed (C) and their interactions AB, AC, BC and ABC are significant, while term radial load (D) and its interactions AD, BD, CD, ABD, ACD, BCD and ABCD are not significant.

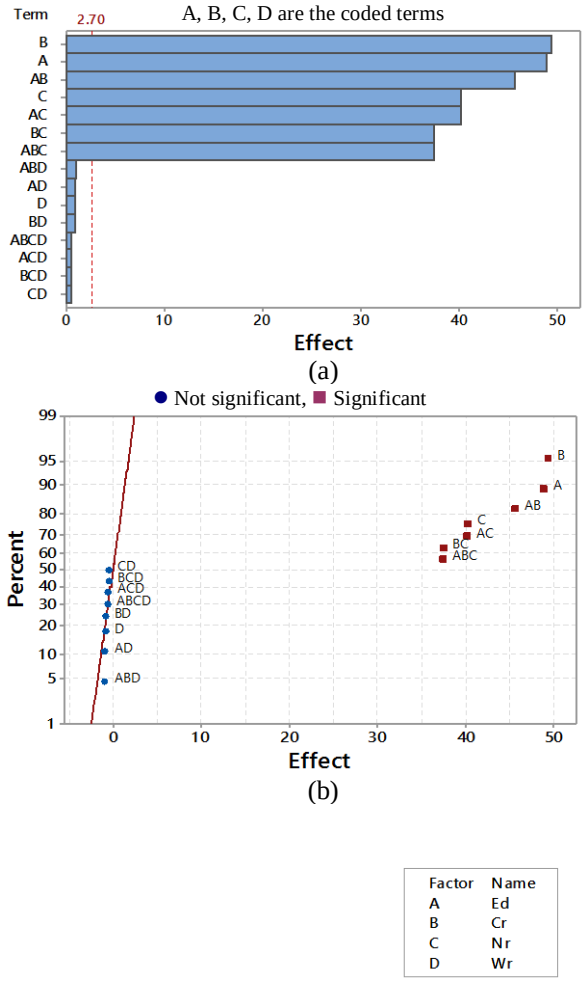

Fig. 11 Pareto chart and normal probability plot of all effects

c) ANOVA Table for Final Model

Pareto chart and normal probability plot show that radial load W_r (D) and its interactions are not significant and hence omitted from the final model. Table VII shows the ANOVA table for the final model (reduced) for response RMS velocity (*Vrms*) of time waveform in the vertical direction. Large model F-value of 3517.57 and small model P-value of zero indicate that the model is highly significant. P-values of main terms E_d, C_r and N_r, are less than 0.05 and are zero, which indicate that these terms are highly significant. Among two way interactions, E_d*C_r, E_d*N_r and C_r*N_r are highly significant, and among three-way interactions, E_d*C_r*N_r is highly significant. The closest value of "R-squared" (0.9997) to 1 and the existence of a good agreement between "Predicated R-squared" (0.9987) with "Adj R-squared" (0.9994) indicates that the model is highly significant.

TABLE VII
ANOVA TABLE FOR VIBRATION RESPONSE IN VERTICAL DIRECTION

Source	dof	Adj SS	Adj MS	F-Value	P-Value
Model	7	51926.9	7418.12	3517.57	0
E_d	1	9570.6	9570.59	4538.24	0
C_r	1	9761.0	9761.02	4628.54	0
N_r	1	6498.1	6498.09	3081.31	0
E_d*C_r	1	8360.9	8360.88	3964.61	0
E_d*N_r	1	6482.9	6482.85	3074.08	0
C_r*N_r	1	5634	5634	2671.57	0
E_d*C_r*N_r	1	5619.4	5619.44	2664.66	0
Error	8	16.9	2.11		
Total	15	51943.7			

d) Regression Equation for Vibration Response in Vertical Direction

Regression equation for vibration response in vertical direction in coded terms is

$$Vrms(V) = 26.611 + 24.457\ E_d + 24.699\ C_r + 20.153\ N_r + 22.859\ E_d{*}C_r + 20.129\ E_d{*}N_r + 18.765\ C_r{*}N_r + 18.741\ E_d{*}C_r{*}N_r$$

Regression equation for vibration response in vertical direction in uncoded terms is

$$Vrms(V) = 0.2453 - 0.9078\ E_d + 0.0691\ C_r - 4.212\times10^{-7}\ N_r - 0.7741\ E_d{*}C_r + 3.608\times10^{-4}\ E_d{*}N_r + 2.5234\times10^{-7}\ C_r{*}N_r + 3.896\times10^{-4}\ E_d{*}C_r{*}N_r$$

e) Performance Prediction

The performance prediction of vibration amplitude in the vertical direction for the final model is shown in the predicted versus actual plot (fig. 12 (a)) and in responses versus observation order graph (fig. 12 (b)). The actual and predicted response values are very close to each other and thus verify the fitness of the polynomial for the response.

f) Main Effect Plots and Interaction Plots

The main effect plot shows the mean response values at each level of input variables. The interaction plot shows the mean response values of two variables at all levels. It helps to understand the behaviour of one variable with respect to another variable. Fig. 13 and fig. 14 show main effect plots and interaction plots for vibration response in the vertical direction (RMS velocity in mm/s) for the final model.

From the main effect plots, it is clear that disk eccentricity (E_d), radial clearance (C_r) and rotor speed (N_r) has a significant positive effect on vibration response. C_r has a greater effect, followed by E_d and N_r. However, radial load (W_r) has a negligible effect (slightly negative) on vibration response.

From the interaction plots, it is clear that significant terms for the vibration response are the interaction between E_d and C_r, E_d and N_r and C_r and N_r. However, there is no interaction seen between E_d and W_r, C_r and W_r, and N_r and W_r. Their interaction lines are absolutely parallel to each other.

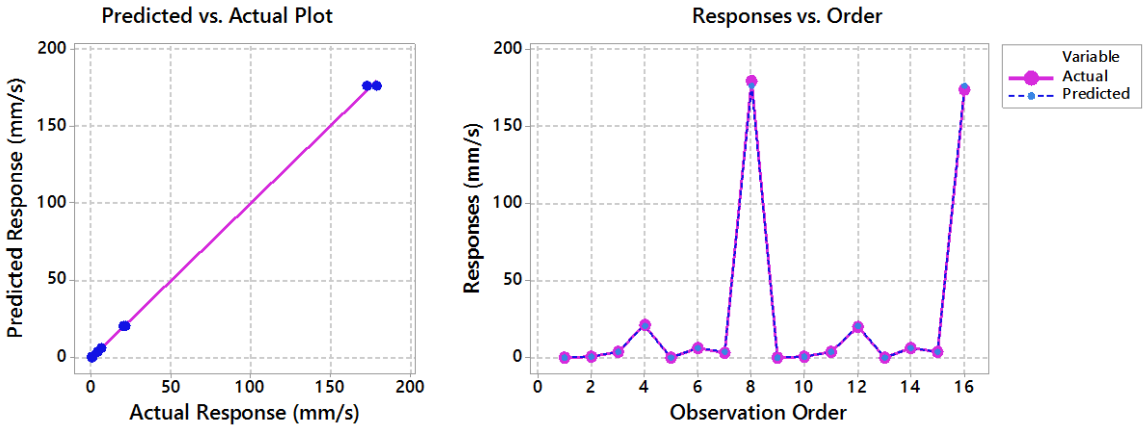

(a) (b)

Fig. 12 Predicted vs actual plot and response vs order plot for vibration response

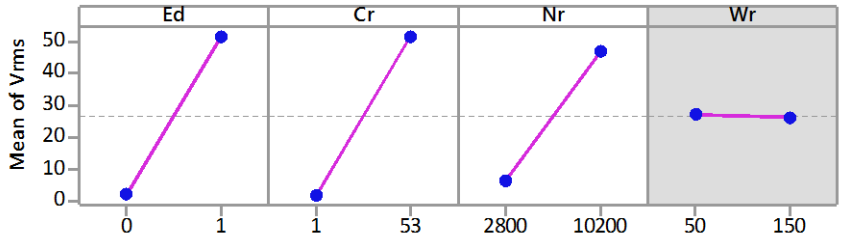

A gray background represents a term not in the model.

Fig. 13 Main effect plots for vibration response in the vertical direction

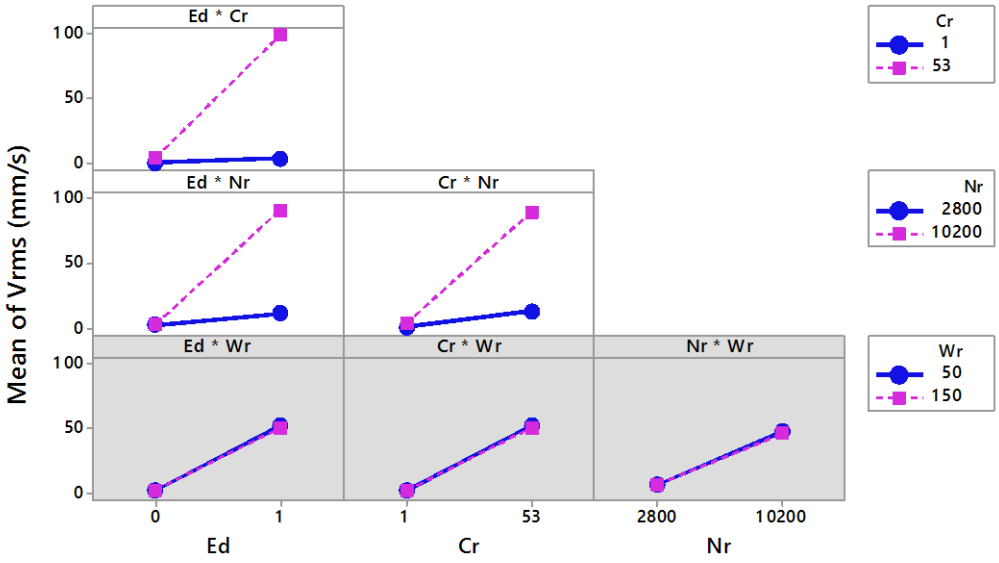

A gray background represents a term not in the model.

Fig. 14 Interaction plots for vibration response in the vertical direction

g) Response Surface Plots

Response surface plot is a 3D plot, which shows the relationship between the response variable and two input variables for the selected range. Fig. 15 shows response surface plots for vibration response in the vertical direction (RMS velocity in mm/s) for two-way interactions of significant factors. Surface plots for interaction between C_r and E_d, N_r and C_r, and N_r and E_d shows that vibration response increases with an increase in values of all these terms (C_r, E_d and N_r) and vibration amplitude is at the highest level when each term reaches their maximum value.

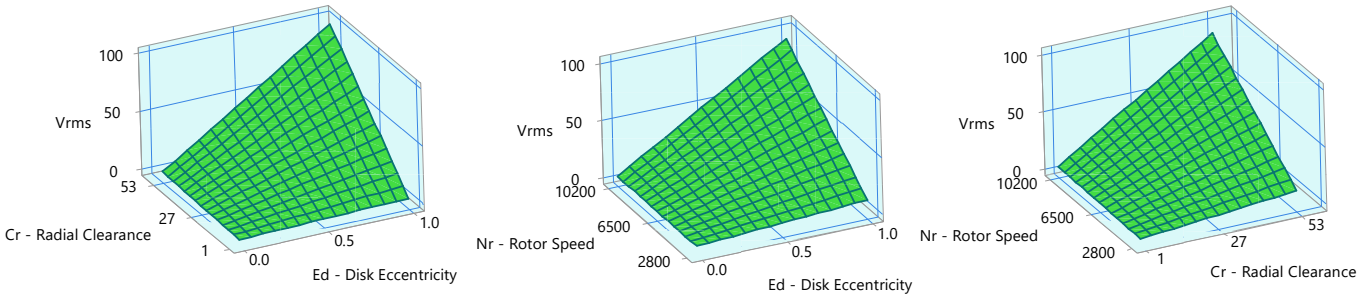

Fig. 15 Response surface plots for vibration response in the vertical direction

1) Effect of disk eccentricity (E_d) on vibration amplitude:

From the main effect plot (fig. 13), it is observed that for an increase in disk eccentricity from 0 to 1 mm, i.e. for the unbalanced rotor, the mean vibration amplitude increases from 2.15 mm/s to 51.06 mm/s, i.e. vibration amplitude increases significantly with increase in disk eccentricity (unbalance).

From interaction plots and surface plots of E_d and C_r (fig. 14), it is observed that at the lowest level of radial clearance (C_r = 1 μm), vibration amplitude increases slightly with an increase in disk eccentricity E_d. At C_r = 1 μm, for increase in E_d from 0 to 1 mm, vibration amplitude increases slightly from 0.31 mm/s to 3.5 mm/s. But, at the highest level of radial clearance (C_r = 53 μm), vibration amplitude increases significantly with an increase in disk eccentricity E_d. At C_r = 53 μm, for increase in E_d from 0 to 1 mm, vibration amplitude increases from 3.99 mm/s to 98.63 mm/s.

From interaction plots and surface plots of E_d and N_r (fig. 14), it is observed that at the lowest level of rotor speed (N_r = 2800 rpm), vibration amplitude increases slightly with an increase in disk eccentricity E_d. At N_r = 2800 rpm, for increase in E_d from 0 to 1 mm, vibration amplitude increases from 2.12 mm/s to 10.78 mm/s. But, at the highest level of rotor speed (N_r = 10200 rpm), vibration amplitude increases significantly with an increase in disk eccentricity E_d. At N_r = 10200 rpm, for increase in E_d from 0 to 1 mm, vibration amplitude increases from 2.17 mm/s to 91.35 mm/s.

2) Effect of radial clearance (C_r) on vibration amplitude:

From the main effect plot (fig. 13), it is observed that for an increase in radial clearance from 1 to 53 μm, the mean vibration amplitude increases from 1.91 mm/s to 51.31 mm/s, i.e. vibration amplitude increases significantly with an increase in radial clearance.

From interaction plots and surface plots of C_r and E_d (fig. 14), it is observed that at the lowest level of disk eccentricity (E_d = 0), i.e. for the balanced rotor, the vibration amplitude increases slightly with the increase in radial clearance C_r. At E_d = 0, for increase in radial clearance from 0 to 53 μm, vibration amplitude increases from 0.31 mm/s to 3.99 mm/s. While at the highest level of disk eccentricity (E_d = 1 mm), i.e. for the unbalanced rotor, the vibration amplitude increases significantly with the increase in radial clearance C_r. At E_d = 1 mm, for increase in radial clearance from 1 to 53 μm, vibration amplitude increases from 3.5 mm/s to 98.63 mm/s.

From interaction plots and surface plots of C_r and N_r (fig. 14), it is observed that at the lowest level of rotor speed (N_r = 2800 rpm), vibration amplitude increases slightly with an increase in radial clearance C_r. At N_r = 2800 rpm, for increase in C_r from 1 to 53 μm, vibration amplitude increases from 0.52 mm/s to 12.39 mm/s. But, at the highest level of rotor speed (N_r = 10200 rpm), vibration amplitude increases significantly with an increase in radial clearance C_r. At N_r = 10200 rpm, for increase in C_r from 1 to 53 μm, vibration amplitude increases from 3.29 mm/s to 90.23 mm/s.

3) Effect of rotor speed (N_r) on vibration amplitude:

From the main effect plot (fig. 13), it is observed that for an increase in rotor speed from 2800 to 10200 rpm, the mean vibration amplitude increases from 6.46 mm/s to 46.76

mm/s, i.e. vibration amplitude increases significantly with an increase in rotor speed.

From interaction plots and surface plots of N_r and E_d (fig. 14), it is observed that at the lowest level of disk eccentricity (E_d = 0), i.e. for the balanced rotor, vibration amplitude increases negligibly with an increase in rotor speed (N_r). At E_d = 0, for increase in rotor speed from 2800 to 10200 rpm, vibration amplitude increases slightly from 2.12 mm/s to 2.17 mm/s (negligible rise). While at the highest level of disk eccentricity (E_d = 1 mm), i.e. for the unbalanced rotor, the vibration amplitude increases significantly with the increase in rotor speed N_r. At E_d = 1 mm, for increase in rotor speed from 2800 to 10200 rpm, vibration amplitude increases from 10.78 mm/s to 91.35 mm/s.

From interaction plots and surface plots of N_r and C_r (fig. 14), it is observed that at the lowest level of radial clearance (C_r = 1 μm), vibration amplitude increases slightly with an increase in rotor speed N_r. At C_r = 1 μm, for increase in N_r from 2800 to 10200 rpm, vibration amplitude increases slightly from 0.52 mm/s to 3.3 mm/s. But, at the highest level of radial clearance (C_r = 53 μm), vibration amplitude increases significantly with an increase in radial speed N_r. At C_r = 53 μm, for increase in N_r from 2800 to 10200 rpm, vibration amplitude increases from 12.39 mm/s to 90.22 mm/s.

h) Contour plots :

The contour plot is a 2D plot, which shows the relationship between the response variable and two input variables for the selected range. Using contour plots, the response amplitude for the specific combination of two input variables in the given range can be determined.

Fig. 16 shows contour plots for vibration response in the vertical direction (RMS velocity in mm/s) for all significant interactions of factors. Contour plots for interaction between C_r and E_d, N_r and C_r, and N_r and E_d shows that vibration response increases with an increase in values of all these terms (C_r, E_d and N_r) and vibration amplitude is at the highest level when each term reaches their maximum value.

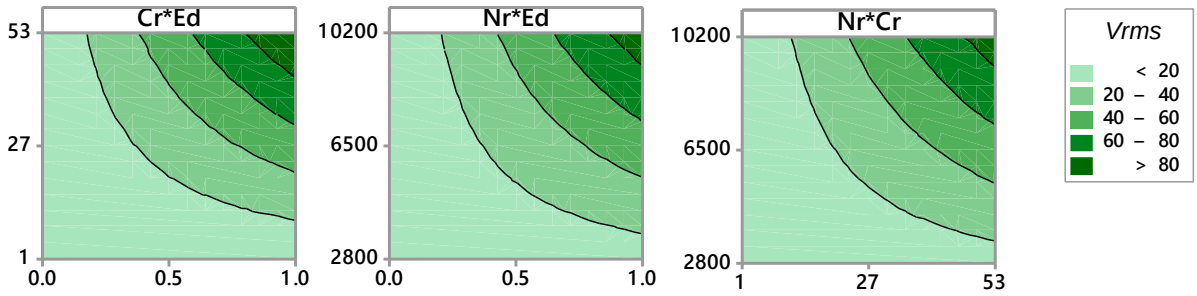

Fig. 16 Contour plots for vibration response in the vertical direction

C. Analysis of Vibration Response in Horizontal Direction using ANOVA

a) ANOVA Table for Final Model

Table VIII shows the ANOVA table for the final model (reduced) for response RMS velocity (*Vrms*) of time waveform in the horizontal direction. Large model F-value of 738.67 and small model P-value of zero indicate that the model is highly significant. P-values of main terms E_d, C_r and N_r, are less than 0.05 and are zero, which indicate that these terms are highly significant. Among two way interactions, E_d*C_r, E_d*N_r and C_r*N_r are highly significant, and among three-way interactions, E_d*C_r*N_r is highly significant. The closest value of "R-squared" (0.9985) to 1 and the existence of a good agreement between "Predicated R-squared" (0.9938) with "Adj R-squared" (0.9971) indicates that the model is highly significant.

TABLE VIII
ANOVA TABLE FOR VIBRATION RESPONSE IN HORIZONTAL DIRECTION

Source	dof	Adj SS	Adj MS	F-Value	P-Value
Model	7	76039.8	10862.8	738.67	0
E_d	1	14189	14189	964.85	0
C_r	1	14300.7	14300.7	972.44	0
N_r	1	9939	9939	675.85	0
E_d*C_r	1	11261.3	11261.3	765.76	0
E_d*N_r	1	10215.7	10215.7	694.67	0
C_r*N_r	1	7932.9	7932.9	539.43	0
E_d*C_r*N_r	1	8201.1	8201.1	557.67	0
Error	8	117.6	14.7		
Total	15	76157.4			

b) Regression Equation for Vibration Response in Horizontal Direction

Regression equation for vibration response in horizontal direction in coded terms is

$$Vrms(H) = 33.244 + 29.779\,E_d + 29.896\,C_r + 24.924\,N_r + 26.530\,E_d{*}C_r + 25.268\,E_d{*}N_r + 22.267\,C_r{*}N_r + 22.640\,E_d{*}C_r{*}N_r$$

Regression equation for vibration response in horizontal direction in uncoded terms is

$$Vrms(H) = -0.11 - 1.72\,E_d + 0.155\,C_r + 1.2\times10^{-5}\,N_r - 1.019\,E_d{*}C_r + 9.5\times10^{-4}\,E_d{*}N_r - 4\times10^{-6}\,C_r{*}N_r + 4.71\times10^{-4}\,E_d{*}C_r{*}N_r$$

c) Main effect plots, Interaction plots, Response surface plots and contour plots

Fig. 17 to fig. 20 shows main effect plots, interaction plots, response surface plots and contour plots for vibration response in the horizontal direction (RMS velocity in mm/s) for the final model. All these plots for vibration response in the horizontal direction look similar to the plots for vibration response in the vertical direction. In main effect plots, the mean vibration amplitudes at higher levels of significant factors E_d, C_r and N_r are 63.02 mm/s, 63.14 mm/s and 58.16 mm/s, respectively. In interaction plots and response surface plots, the higher mean vibration amplitudes for interactions between E_d and C_r, E_d and N_r, and C_r and N_r are 119.45 mm/s, 113.21mm/s and 110.33 mm/s, respectively. It is observed that at higher levels of significant factors E_d, C_r and N_r, the vibration amplitudes for horizontal vibration responses are higher than that of vertical vibration responses.

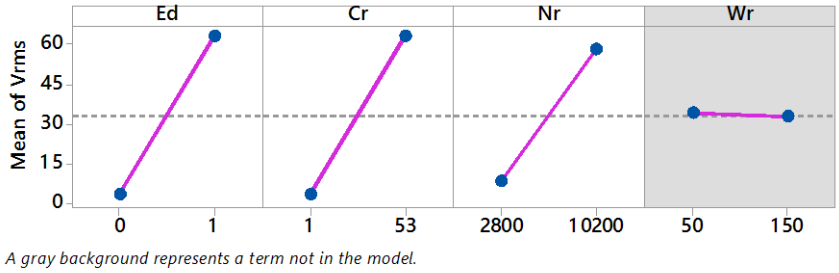

Fig. 17 Main effect plots for vibration response in the horizontal direction

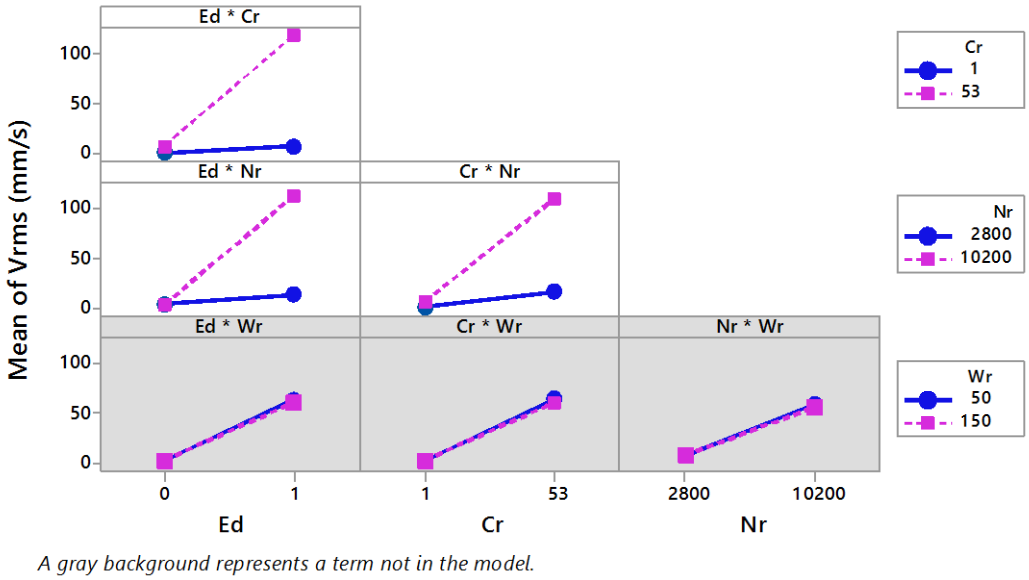

Fig. 18 Interaction plots for vibration response in the horizontal direction

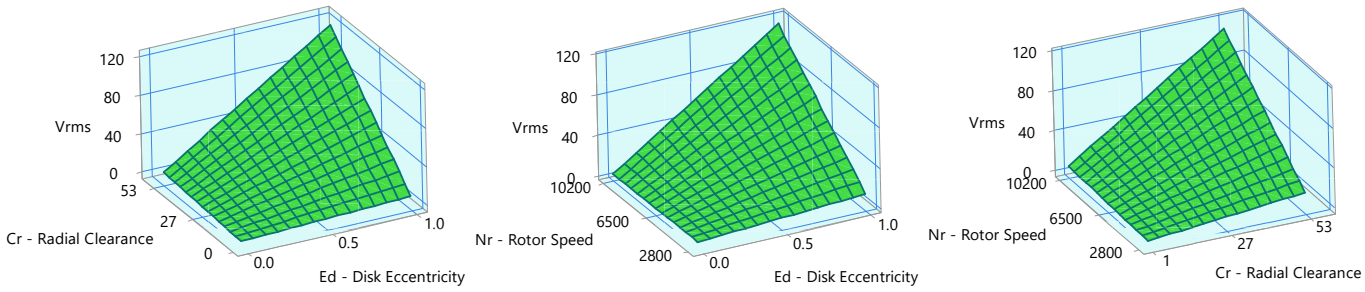

Fig. 19 Response surface plots for vibration response in the horizontal direction

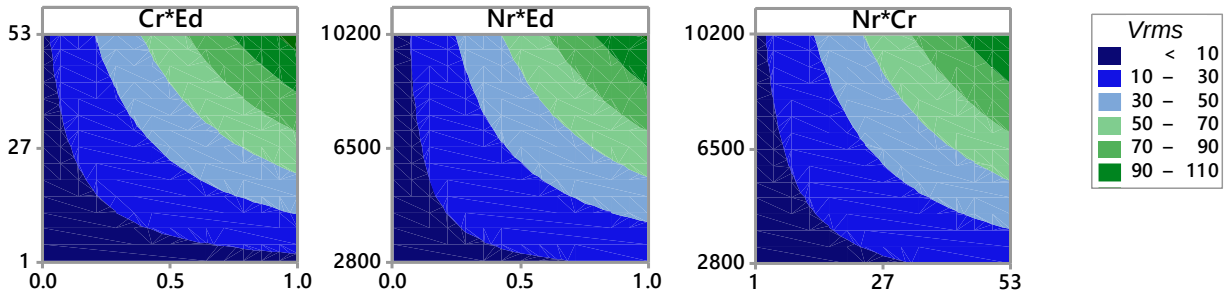

Fig. 20 Contour plots for vibration response in the horizontal direction

IV. CONCLUSIONS

In the present work, COMSOL multiphysics software is used for modelling and simulation of vibrations in a rotor-bearing system. 2-level FFD and response surface analysis methods are used to study and analyze the effects of four factors, namely disk eccentricity (for balanced/unbalanced rotor), radial clearance, rotor speed and radial load on vibration amplitude in vertical and horizontal directions of a rotor-bearing system having 6205 ball bearings at both ends of the rotor. Regression equations are developed to predict the vibration responses at a ball bearing, and response surfaces are obtained, which depict the effects of input variables on vibration responses. From the analysis of vibration responses for the selected range of factors, the following conclusions can be drawn:

1) Radial clearance of the bearing has a remarkable effect on vibration response of rotor-bearing system followed by disk eccentricity (which causes unbalance) and rotor speed, and radial load on bearing has no significant effect on vibration response of the rotor-bearing system.
2) Radial clearance, disk eccentricity and rotor speed cause low vibration amplitudes at their lower levels and very high vibration amplitudes at their higher levels. Interaction plots and response surface plots between these factors show similar characteristics but are indifferent in magnitude.
3) Vibration amplitude increases due to disk eccentricity and rotor speed because, in combination, these factors raise centrifugal forces on the rotor. The radial clearance allows extra displacement of the inner race and balls and hence increases vibration.
4) Time waveforms of balanced rotor clearly show the peaks are found at intervals that correspond to critical speed frequency. Hence, time waveforms of the balanced rotor can be used to determine the critical speed of the rotor.
5) The centre of the balanced rotor displaces in a downward direction due to radial load and vibrates there in vertical and horizontal directions only. At the same time, the centre of the unbalanced rotor rotates about the initial position due to centrifugal force.
6) An unbalanced rotor becomes more unstable with an increase in clearance and speeds the system. For unbalanced rotors, at low clearance, the only dominant frequencies are the synchronous frequencies at f_c and f_r, and with the increase in clearance, the non-synchronous frequencies increase.
7) Vibration responses in the vertical and horizontal direction show similar characteristics but are different in magnitudes. Vibration amplitudes in the vertical direction are smaller than in the horizontal direction. This is due to radial load, which is acting in the vertical direction.

APPENDICES

Appendix A: Calculation of Linear Bearing Stiffness Coefficient K

According to Hertzian contact theory, the geometry of point contact between a race and a ball is described by four radii of curvature. By definition, convex surfaces have positive radii, and concave surfaces have negative radii [41].

For inner race and ball contact :

Fig. A1 shows the geometry of point contact between the inner race and a ball with four radii of curvature. Four radii of curvatures of contacting surfaces of the inner race and a ball in X and Y directions can be calculated using the following relations

Radii of curvature of the ball in X and Y directions

$$r_{bX} = r_{bY} = \frac{D_b}{2} = \frac{7.94}{2} = 3.97 \text{ mm}$$

Radii of curvature of inner race in X and Y directions

$$r_{iX} = -r_i = -4.2082 \text{ mm}$$

$$r_{iY} = \frac{D_i}{2} = \frac{31.10}{2} = 15.55 \text{ mm}$$

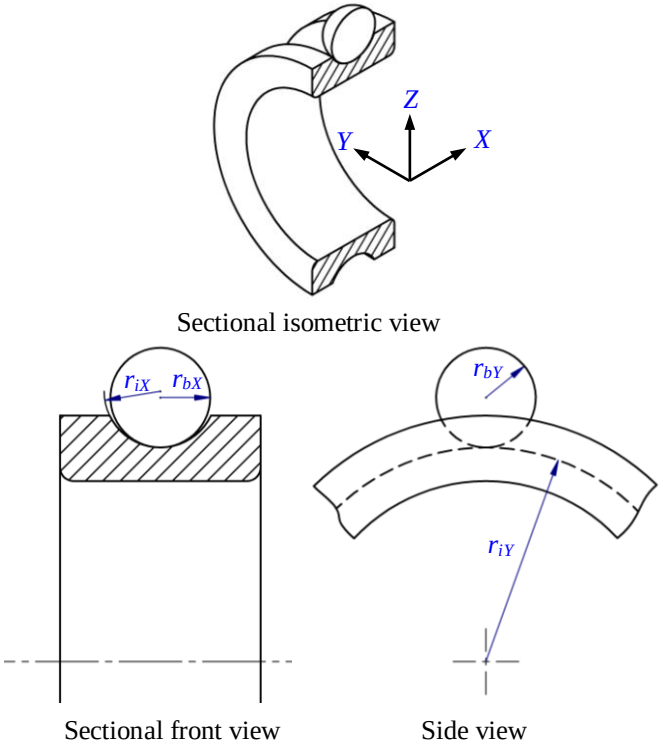

Sectional isometric view

Sectional front view Side view

Fig. A1 Inner race and ball in contact with four radii of curvature

Two effective radii of curvatures of the contacting surfaces R_X and R_Y in X and Y directions can be calculated using following relations

$$\frac{1}{R_X} = \frac{1}{r_{bX}} + \frac{1}{r_{iX}} \quad \text{and} \quad \frac{1}{R_Y} = \frac{1}{r_{bY}} + \frac{1}{r_{iY}}$$

$$\therefore \quad R_X = \frac{1}{\frac{1}{r_{bX}} + \frac{1}{r_{iX}}} = \frac{1}{\frac{1}{3.97} + \frac{1}{-4.2082}} = 70.136 \text{ mm}$$

$$\text{and} \quad R_Y = \frac{1}{\frac{1}{r_{bY}} + \frac{1}{r_{iY}}} = \frac{1}{\frac{1}{3.97} + \frac{1}{15.55}} = 3.1625 \text{ mm}$$

The combined radius of curvature R of the contacting surfaces can be calculated using the following relation

$$\frac{1}{R} = \frac{1}{R_X} + \frac{1}{R_Y}$$

$$\therefore \quad R = \frac{1}{\frac{1}{R_X} + \frac{1}{R_Y}} = \frac{1}{\frac{1}{70.136} + \frac{1}{3.1625}} = 3.026 \text{ mm}$$

$$= 0.003026 \text{ m}$$

The contact stiffness for point contact between inner race and ball K_{cin} is given as

$$K_{cin} = \pi k_e E'_{in} \sqrt{\frac{R\xi}{4.5\,\zeta^3}}$$

where E'_{in} is the equivalent modulus of elasticity between inner race and ball, which can be calculated from the following equation

$$E'_{in} = \frac{2}{\left(\frac{1-\nu_{inner}^2}{E_{inner}} + \frac{1-\nu_{ball}^2}{E_{ball}}\right)}$$

In which ν_{inner} and ν_{ball} are the Poisson's ratio of inner race and ball materials; and E_{inner} and E_{ball} are Young's modulus of the inner race and ball materials.

$$\therefore \quad E'_{in} = \frac{2}{\left(\frac{1-0.3^2}{200} + \frac{1-0.3^2}{200}\right)} = 219.78022 \text{ GPa}$$

$$= 219.78022 \times 10^9 \text{ N/m}^2$$

as, $\nu_{inner} = \nu_{ball} = 0.3$ and $E_{inner} = E_{ball} = 200$ GPa.

And ζ and ξ are 1st and 2nd kind of elliptical integral and k_e is the ellipticity parameter. Their approximate values are

$$\zeta = 1.5277 + 0.6023 \ln\left(\frac{R_2}{R_1}\right)$$

$$= 1.5277 + 0.6023 \ln\left(\frac{70.136}{3.1625}\right) = 3.394262975$$

$$\xi = 1.0003 + 0.5968\left(\frac{R_1}{R_2}\right)$$

$$= 1.0003 + 0.5968\left(\frac{3.1625}{70.136}\right) = 1.027210687$$

$$k_e = 1.0339\left(\frac{R_2}{R_1}\right)^{0.6360} = 1.0339\left(\frac{70.136}{3.1625}\right)^{0.6360}$$

$$= 7.421189$$

$$\therefore \quad K_{cin} = \pi k_e E'_{in}\sqrt{\frac{R\xi}{4.5\,\zeta^3}}$$

$$= \pi \times 7.421189 \times 219.78022 \times 10^9 \times \sqrt{\frac{0.003026 \times 1.027210687}{4.5 \times 3.394262975^3}}$$

$$\therefore \quad \boldsymbol{K_{cin} = 2.153578033920 \times 10^{10}\ \text{N/m}}$$

For outer race and ball contact :

Fig. A2 shows the geometry of point contact between the outer race and a ball with four radii of curvature.

Four radii of curvatures of contacting surfaces of the outer race and a ball in X and Y directions can be calculated using the following relations.

Radii of curvature of ball in X and Y directions

$$r_{bX} = r_{bY} = \frac{D_b}{2} = \frac{7.94}{2} = 3.97 \text{ mm}$$

Radii of curvature of outer race in X and Y directions

$$r_{oX} = -r_o = -4.2082 \text{ mm}$$

$$r_{oY} = -\frac{D_o}{2} = -\frac{46.98}{2} = -23.49 \text{ mm}$$

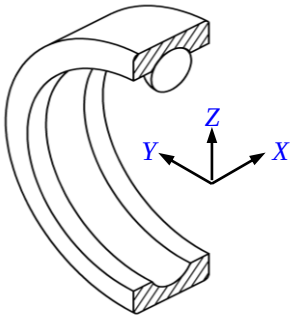

Sectional isometric view

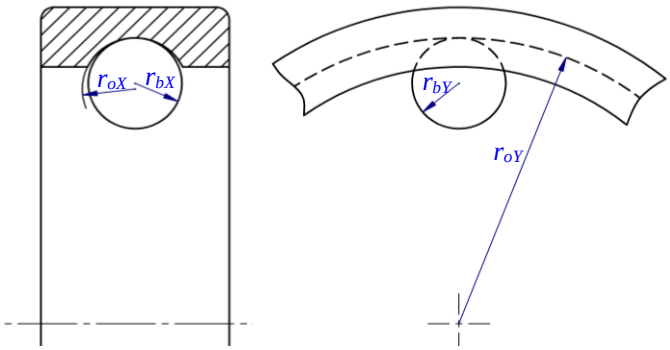

Sectional front view Side view

Fig. A2 Outer race and ball in contact with four radii of curvature

Two effective radii of curvatures of the contacting surfaces R_X and R_Y in X and Y directions can be calculated using the following relations

$$\frac{1}{R_X} = \frac{1}{r_{bX}} + \frac{1}{r_{iX}} \quad \text{and} \quad \frac{1}{R_Y} = \frac{1}{r_{bY}} + \frac{1}{r_{iY}}$$

$$\therefore \quad R_X = \frac{1}{\frac{1}{r_{bX}} + \frac{1}{r_{iX}}} = \frac{1}{\frac{1}{3.97} + \frac{1}{-4.2082}} = 70.136 \text{ mm}$$

$$\text{and} \quad R_Y = \frac{1}{\frac{1}{r_{bY}} + \frac{1}{r_{iY}}} = \frac{1}{\frac{1}{3.97} + \frac{1}{-23.49}} = 4.777 \text{ mm}$$

The combined radius of curvature R of the contacting surfaces can be calculated using the following relation

$$\frac{1}{R} = \frac{1}{R_X} + \frac{1}{R_Y}$$

$$\therefore \quad R = \frac{1}{\frac{1}{R_X} + \frac{1}{R_Y}} = \frac{1}{\frac{1}{70.136} + \frac{1}{4.777}} = 4.7272 \text{ mm}$$

$$= 0.0044727 \text{ m}$$

The contact stiffness for point contact between outer race and ball K_{cout} is given as

$$K_{cout} = \pi k_e E'_{out}\sqrt{\frac{R\xi}{4.5\,\zeta^3}}$$

where E'_{out} is the equivalent modulus of elasticity between outer race and ball, which can be calculated from the following equation

$$E'_{out} = \frac{2}{\left(\frac{1-\nu_{outer}^2}{E_{outer}} + \frac{1-\nu_{ball}^2}{E_{ball}}\right)}$$

In which ν_{outer} and ν_{ball} are the Poisson's ratio of the outer race and ball materials, and E_{outer} E_{ball} are Young's modulus of the outer race and ball materials.

$$E'_{out} = \frac{2}{\left(\frac{1-0.3^2}{200} + \frac{1-0.3^2}{200}\right)}$$

$$= 219.78022 \text{ GPa} = 219.78022 \times 10^9 \text{ N/m}^2$$

as, $\nu_{outer} = \nu_{ball} = 0.3$ and $E_{outer} = E_{ball} = 200$ GPa.

And ζ ξ are the first and second kinds of elliptical integral and k_e is the ellipticity parameter. Their approximate values are

$$\zeta = 1.5277 + 0.6023 \ln\left(\frac{R_2}{R_1}\right)$$

$$= 1.5277 + 0.6023 \ln\left(\frac{70.136}{4.777}\right) = 3.145805696$$

$$\xi = 1.0003 + 0.5968\left(\frac{R_1}{R_2}\right)$$

$$= 1.0003 + 0.5968\left(\frac{4.777}{70.136}\right)$$

$$= 1.040951577$$

$$k_e = 1.0339\left(\frac{R_2}{R_1}\right)^{0.6360}$$

$$= 1.0339\left(\frac{70.136}{4.777}\right)^{0.6360}$$

$$= 5.708637$$

$$\therefore K_{cout} = \pi k_e E'_{out}\sqrt{\frac{R\xi}{4.5\,\zeta^3}}$$

$$= \pi \times 5.708637 \times 219.78022 \times 10^9 \times \sqrt{\frac{0.0044727 \times 1.040951577}{4.5 \times 3.145805696^3}}$$

$$\therefore \boldsymbol{K_{cout} = 2.27232128434 \times 10^{10}\ \text{N/m}}$$

The equivalent contact stiffness K corresponding to both inner and outer contacts is

$$K = \frac{1}{\left[\left(\frac{1}{K_{cin}}\right)^{\frac{2}{3}} + \left(\frac{1}{K_{cout}}\right)^{\frac{2}{3}}\right]^{\frac{3}{2}}}$$

$$= \frac{1}{\left[\left(\frac{1}{2.153578033920 \times 10^{10}}\right)^{\frac{2}{3}} + \left(\frac{1}{2.27232128434 \times 10^{10}}\right)^{\frac{2}{3}}\right]^{\frac{3}{2}}}$$

$$\therefore \quad \boldsymbol{K = 7.819265042099 \times 10^9\ \text{N/m}}$$

Appendix B: Calculation of Radial Loads (W_r) on each bearing

Fig. B1 shows the rotor with disk simply supported between two ball bearings, and fig. B2 shows the rotor as a simply supported beam subjected to loads due to rotor and disk weights. If W_{ro} and W_d are the weight of rotor and disk, respectively, then the radial load on each bearing W_r will be equal to the reactions at each bearing end.

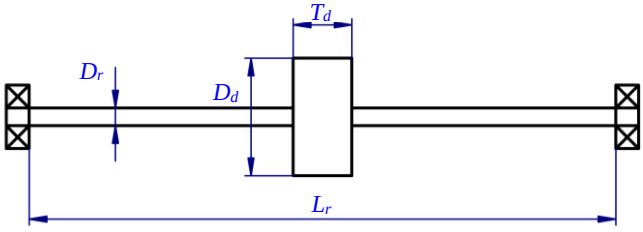

Fig. B1. Rotor with disk supported between bearings

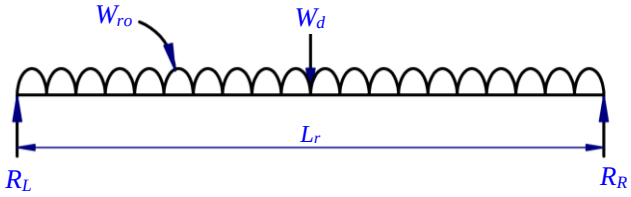

Fig. B2. Loads acting on the rotor

Calculation of radial load on each bearing (W_r) :

Mass of rotor (m_{ro}) = Density × Volume

= Density × (Area × Length)

$$= \rho \times \left(\frac{\pi}{4} D_r^{\,2} \times L_r\right) = 7850 \times \left(\frac{\pi}{4} 0.025^{\,2} \times 1\right)$$

= 3.85336 kg

Weight of rotor (W_{ro}) = Mass of rotor × gravitational acce^{n}

$= m_{ro} \times g$ = 3.85336 × 9.81 = 37.8 N

For disk thickness 26.12 mm :

Mass of disk (m_d) = Density × Volume

= Density × (Area × Thickness)

$$= \rho \times \left(\frac{\pi}{4}(D_d^{\,2} - D_r^{\,2}) \times T_d\right)$$

$$= 7850 \times \left(\frac{\pi}{4}(0.2^2 - 0.025^2) \times 0.02612\right)$$

= 6.3409 kg

Weight of disk (W_d) = Mass of disk × gravitational acce^{n}

$= m_d \times g$ = 6.3409 × 9.81 = 62.2 N

Total weight of rotor & disk (W) = W_{ro} + W_d

= 37.8 + 62.2 = 100 N

Radial load on each bearing (W_r) = Reactions at each end

$$= \frac{W}{2} = \frac{100}{2} = 50\ \text{N}$$

For disk thickness 110.09 mm :

Mass of disk (m_d) = Density × Volume

= Density × (Area × Thickness)

$$= \rho \times \left(\frac{\pi}{4}(D_d^{\,2} - D_r^{\,2}) \times T_d\right)$$

$$= 7850 \times \left(\frac{\pi}{4}(0.2^2 - 0.025^2) \times 0.11009\right)$$

= 26.7276 kg

Weight of disk (W_d) = Mass of disk × gravitational acce^{n}

$= m_d \times g$ = 26.7276 × 9.81 = 262.2 N

Total weight of rotor & disk (W) = W_{ro} + W_d

= 37.8 + 262.2 = 300 N

Radial load on each bearing (W_r) = Reactions at each end

$$= \frac{W}{2} = \frac{300}{2} = 150\ \text{N}$$

Appendix C: Critical speeds of rotor obtained for the selected radial loads and radial clearances

Table C1 shows the values of linear bearing stiffness coefficient K and critical speeds N_c (critical frequencies f_c) obtained for selected values of radial loads (W_r) and radial clearances (C_r) using COMSOL and Dyrobes simulators. Critical speed values for the first three modes are given in the table.

TABLE C1
Values of K and N_c (f_c) were obtained for given W_r and C_r using simulators

Radial load (W_r) in Newton	Stiffness coefficient and Critical speeds	Radial clearances in μm	
		1 μm	53 μm
50	K in N/m	$7.8192650338868 \times 10^9$	$7.8192646068505 \times 10^9$
	N_c (f_c) in rpm (Hz)	1428.07 (23.80) 1428.32 (23.80) 7708.71 (128.48)	1428.07 (23.80) 1428.32 (23.80) 7708.71 (128.48)
150	K in N/m	$7.8192650338868 \times 10^9$	$7.8192646068505 \times 10^9$
	N_c (f_c) in rpm (Hz)	765.55 (12.759) 795.59 (12.76) 4096.24 (68.27)	765.55 (12.759) 795.59 (12.76) 4096.24 (68.27)

Appendix D: Calculation of critical speed by analytical method

Fig. D1 shows the rotor as a simply supported beam subjected to rotor weight W_{ro} and disk weight W_d.

Static deflection of the rotor δ_{rr} due to uniformly distributed rotor weight W_{ro}

$$\delta_{rr} = \frac{5W_{ro}L_r^4}{384E_rI_r} = \frac{5\times37.8\times1^4}{384\times200\times10^9\times\frac{\pi}{64}0.025^4}$$

$$= 1.2834\times10^{-4}\text{ m}$$

For disk thickness 26.12 mm :

For T_d = 26.12 mm and D_d = 0.2 m, disk weight W_d = 62.2 N (see annexure B).

Static deflection of the rotor δ_{rd} due to concentrated mid-point disk weight W_d

$$\delta_{rd} = \frac{W_dL_r^3}{48E_rI_r} = \frac{62.2\times1^3}{48\times200\times10^9\times\frac{\pi}{64}0.025^4}$$

$$= 3.379\times10^{-4}\text{ m}$$

Total static deflection of the rotor δ_r due to disk weight W_d and rotor weight W_{ro}

$$\delta_r = \delta_{rr} + \delta_{rd}$$
$$= 1.2834\times10^{-4} + 3.379\times10^{-4}$$
$$= 4.6624\times10^{-4}\text{ m}$$

Natural angular frequency of the rotor ω_n

$$\omega_n = \sqrt{\frac{g}{\delta_r}} = \sqrt{\frac{9.81}{4.6624\times10^{-4}}} = 145.054\text{ rad/s}$$

Critical speed of the rotor N_c

$$N_c = \frac{\omega\times60}{2\pi} = \frac{145.054\times60}{2\pi} = 1385.16\text{ rpm}$$

Critical frequency of the rotor f_c

$$f_c = \frac{N_c}{60} = \frac{1385.16}{60} = 23.09\text{ Hz}$$

For disk thickness 110.09 mm :

For T_d = 119.09 mm and D_d = 0.2 m, disk weight W_d = 262.2 N (see annexure B).

Static deflection of the rotor δ_{rd} due to concentrated mid-point disk weight W_d

$$\delta_{rd} = \frac{W_dL_r^3}{48E_rI_r} = \frac{262.2\times1^3}{48\times200\times10^9\times\frac{\pi}{64}0.025^4}$$

$$= 1.4244\times10^{-3}\text{ m}$$

Total static deflection of the rotor δ_r due to disk weight W_d and rotor weight W_{ro}

$$\delta_r = \delta_{rr} + \delta_{rd}$$
$$= 1.2834\times10^{-4} + 1.4244\times10^{-3}$$
$$= 1.5527\times10^{-3}\text{ m}$$

Natural angular frequency of the rotor ω_n

$$\omega_n = \sqrt{\frac{g}{\delta_r}} = \sqrt{\frac{9.81}{1.5527\times10^{-3}}} = 79.485\text{ rad/s}$$

Critical speed of the rotor N_c

$$N_c = \frac{\omega\times60}{2\pi} = \frac{79.485\times60}{2\pi} = 759.03\text{ rpm}$$

Critical frequency of the rotor f_c

$$f_c = \frac{N_c}{60} = \frac{759.03}{60} = 12.65\text{ Hz}$$

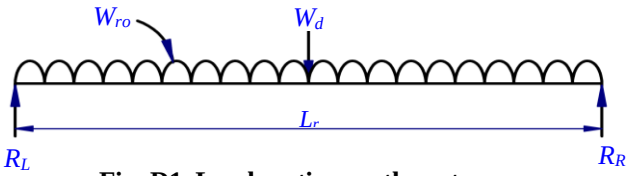

Fig. D1. Loads acting on the rotor

ACKNOWLEDGEMENTS

The authors are gratefully acknowledged to Maharashtra Institute of Technology Aurangabad and T.P.C.T's College of Engineering Osmanabad for providing a literature survey facility and licensed software for this work.

REFERENCES

[1] F. B. Oswald, E. V. Zaretsky, and J. V. Poplawski, Effect of Internal Clearance on Load Distribution and Life of Radially Loaded Ball and Roller Bearings, Tribology Transactions, 55(2) (2012) 245–265.

[2] P. Zmarzly, Influence of the Internal Clearance of Ball Bearings on the Vibration Level, presented at the 24th International Conference Engineering Mechanics, Svratka, Czech Republic, (2018).

[3] W. Jing, Non-synchronous Vibration due to Internal Radial Clearance in Roller Bearings, M.E. Dissertation Thesis, McGill University Montreal, Canada, (2010).

[4] D. P. Fleming, B. Murphy, J. Sawicki, and J. V. Poplawski, Transient Response of Rotor on Rolling-Element Bearings with Clearance, presented at the 7th IFToMM Conference on Rotor Dynamics, Vienna, Austria, (2006).

[5] I. M. Jamadar, A Model to Estimate Synchronous Vibration Amplitude for Detection of Unbalance in Rotor-Bearing System, The Int. Journal of Acoustics and Vibration, 26(2) (2021) 161–169.

[6] P. H. Jain and S. P. Bhosle, Analysis on Vibration Signal Analysis Techniques used in Diagnosis of Faults in Rotating Machinery, International Journal of Mechanical and Production Engineering Research and Development, 10(3) (2020) 3377–3396.

[7] P. H. Jain and S. P. Bhosle, A Review on Vibration Signal Analysis Techniques Used for Detection of Rolling Element Bearing Defects, SSRG International Journal of Mechanical Engg., 8(1) (2021) 14-29.

[8] M. Tiwari, K. Gupta, and O. Prakash, Effect of Radial Internal Clearance of a Ball Bearing on the Dynamics of a Balanced Horizontal Rotor, Journal of Sound and Vibration, 238 (5) (2000) 723–756.

[9] M. Tiwari, K. Gupta, and O. Prakash, Dynamic Response of an Unbalanced Rotor Supported on Ball Bearings, Journal of Sound and Vibration, 238 (5) (2000) 757–779.

[10] S. P. Harsha, Rolling Bearing Vibrations—The Effects of Surface Waviness and Radial Internal Clearance, Int. Journal for Comp. Methods in Engg Science and Mechanics, 7(2) (2006) 91–111.

[11] S. P. Harsha, Nonlinear Dynamic Analysis of a High-speed Rotor Supported by Rolling Element Bearings, Journal of Sound and Vibration, 290(1) (2006) 65–100.

[12] S. P. Harsha, Nonlinear Dynamic Analysis of an Unbalanced Rotor Supported by Roller Bearing, Chaos, Solitons & Fractals, 26 (1) (2005) 47–66.

[13] B. Changqing and X. Qingyu, Dynamic Model of Ball Bearings with Internal Clearance and Waviness, Journal of Sound and Vibration, 294(1) (2006) 23–48.

[14] S. H. Upadhyay, S. P. Harsha, and S. C. Jain, Analysis of Nonlinear Phenomena in High-Speed Ball Bearings due to Radial Clearance and Unbalanced Rotor Effects, Journal of Vibration and Control, 16(1) (2010) 65–88.

[15] G. Chen, Study on Nonlinear Dynamic Response of an Unbalanced Rotor Supported on Ball Bearing, Journal of Vibration and Acoustics, 131(6) (2009) 061001(9p).

[16] K. Kappaganthu and C. Nataraj, Nonlinear Modeling and Analysis of a Rolling Element Bearing with a Clearance, Communications in Nonlinear Sci. and Numerical Simulation, 16(10) (2011) 4134–4145.

[17] G. Nan, M. Tang, E. Chen, and A. Yang, Nonlinear Dynamic Mechanism of Rolling Element Bearings with an Internal Clearance in a Rotor-bearing System, Advances in Mechanical Engg., 8(11) (2016).

[18] H. Cheng, Y. Zhang, W. Lu, and Z. Yang, Mechanical Characteristics and Nonlinear Dynamic Response Analysis of Rotor-bearing-coupling System, Applied Mathematical Modelling, 93 (2021) 708–727.

[19] M. Xu, G. Feng, Q. He, F. Gu, and A. Ball, Vibration Characteristics of Rolling Element Bearings With Different Radial Clearances for Condition Monitoring of Wind Turbine, Applied Sciences, 10 (14) (2020) 14.

[20] P. H. Jain and S. P. Bhosle, Study of Effects of Radial Load on Vibration of Bearing using Time-domain Statistical Parameters, IOP Conf. Series, Materials Science and Engg., 1070 (2021) 012130 (14).

[21] Z. Kiral and H. Karagülle, Simulation and Analysis of Vibration Signals Generated by Rolling Element Bearing with Defects, Tribology International, 36(9) (2003) 667–678.

[22] Z. Kıral and H. Karagülle, Vibration Analysis of Rolling Element Bearings With Various Defects under the Action of an Unbalanced Force, Mech. Systems and Signal Processing, 20(8) (2006) 1967–1991.

[23] J. Liu, Y. Shao, and M. J. Zuo, The effects of the shape of the localized defect in ball bearings on the vibration waveform, Proceedings of the Institution of Mechanical Engineers, Part K, Journal of Multi-body Dynamics, 227(3) (2013) 261-274.

[24] S. Singh, U. G. Köpke, C. Q. Howard, and D. Petersen, Analyses of Contact Forces and Vibration Response for a Defective Rolling Element Bearing using an Explicit Dynamics Finite Element Model, Journal of Sound and Vibration, 333(21) (2014) 5356–5377.

[25] S. Tyagi and S. K. Panigrahi, Transient Analysis of Ball Bearing Fault Simulation using Finite Element Method, J. Inst. Eng. India Ser. C, 95(4) (2014) 309–318.

[26] A. Nabhan, M. Nouby, A. Sami, and M. Mousa, Vibration Analysis of Deep Groove Ball Bearing with Outer Race Defect using ABAQUS, Journal of Low-Frequency Noise, Vibration and Active Control, 35(4) (2016) 312–325.

[27] X. Yang, C. Yan, and Y. Li, Finite Element Simulation and Experimental Study on Vibration Effect of Defect Position for Cylindrical Roller Bearing, 10(8) (2017) 1–12.

[28] P. K. Kankar, S. P. Harsha, P. Kumar, and S. C. Sharma, Fault Diagnosis of a Rotor Bearing System using Response Surface Method, European Journal of Mechanics - A/Solids, 28(4) (2009) 841–857.

[29] M. Patil, J. Mathew, P. Rajendrakumar, and S. Karade, Experimental Studies Using RSM for Condition Monitoring of Ball Bearings, Journal of Tribology, 132(4) (2010) 044505(6p).

[30] P. K. Kankar, S. C. Sharma, and S. P. Harsha, Fault Diagnosis of High-Speed Rolling Element Bearings Due to Localized Defects Using Response Surface Method, Journal of Dynamic Systems, Measurement, and Control, 133(3) (2011) 031007(14).

[31] P. K. Kankar, S. C. Sharma, and S. P. Harsha, Vibration Signature Analysis of a High-Speed Rotor Supported on Ball Bearings due to Localized Defects, Journal of Vibration and Control, 19(12) (2012) 1833–1853.

[32] I. M. Jamadar and D. P. Vakharia, An In-situ Synthesized Model for Detection of Defective Roller in Rolling Bearings, Engineering Science and Technology, an Int. Journal, 19(3) (2016) 1488–1496.

[33] E. Yucel and H. Saruhan, Design Optimization of Rotor-bearing System Considering Critical Speed Using Taguchi Method, Proceedings of the Institution of Mechanical Engineers, Part E, Journal of Process Mechanical Engineering, 231(2) (2017) 138–146.

[34] M. Boumahdi, S. Rechak, and S. Hanini, Analysis and Prediction of Defect Size and Remaining Useful Life of Thrust Ball Bearings, Modelling and Experiment Procedures, Arab J Sci Eng, 42(11) (2017) 4535–4546.

[35] V. R. Patil and P. V. Jadhav, Dynamic Response Analysis of Unbalanced Rotor-bearing System with Internal Radial Clearance, SN Appl. Sci., 2(11) (2020) 1826(1-13).

[36] P. Patra, V. H. Saran, and S. Harsha, Vibration Response Analysis of High-speed Cylindrical Roller Bearings Using Response Surface Method, Proceedings of the Institution of Mechanical Engineers, Part K, Journal of Multi-body Dynamics, 234(2) (2020) 379–392.

[37] P. Singh and S. P. Harsha, Vibration Response-Based Fault Diagnosis of Cylindrical Roller Bearing Using Response Surface Methodology, Journal of Nondestructive Evaluation, Diagnostics and Prognostics of Engineering Systems, 3(2) (2020) 0212002(23).

[38] H. P. Mishra and A. Jalan, Analysis of Faults in Rotor-bearing System Using Three-level Full Factorial Design and Response Surface Methodology, Noise & Vibration Worldwide, 52(11) (2021) 365-376.

[39] S. Patil, A. K. Jalan, and A. M. Marathe, Experimental Investigation Using RSM for Condition Monitoring of Misaligned Rotor System, Journal of Nondestructive Evaluation, Diagnostics and Prognostics of Engineering Systems, 5(2) (2021) 021003(10).

[40] Modelling Rotordynamics in COMSOL Multiphysics®, COMSOL. https,//www.comsol.co.in/video/modeling-rotordynamics-in-comsol-multiphysics (accessed Nov. 19, 2021).

[41] T. A. Harris, Rolling Bearing Analysis, 4th ed. John Wily and Son, INC., 2001.

[42] K.M. Arunkumar and T.C. Manjunath, A Brief Review/Survey of Vibration Signal Analysis in Time Domain, SSRG International Journal of Electronics and Communication Engg., 3(3) (2016) 12–15.